

Spectral rate theory for projected two-state kinetics

Jan-Hendrik Prinz,¹ John D. Chodera,² and Frank Noé^{1,*}

¹DFG Research Center Matheon, Free University Berlin, Arnimallee 6, 14195 Berlin, Germany[†]

²Computational Biology Program, Memorial Sloan-Kettering Cancer Center, New York, NY 10065, USA[‡]

Classical rate theories often fail in cases where the observable(s) or order parameter(s) used are poor reaction coordinates or the observed signal is deteriorated by noise, such that no clear separation between reactants and products is possible. Here, we present a general spectral two-state rate theory for ergodic dynamical systems in thermal equilibrium that explicitly takes into account how the system is observed. The theory allows the systematic estimation errors made by standard rate theories to be understood and quantified. We also elucidate the connection of spectral rate theory with the popular Markov state modeling (MSM) approach for molecular simulation studies. An optimal rate estimator is formulated that gives robust and unbiased results even for poor reaction coordinates and can be applied to both computer simulations and single-molecule experiments. No definition of a dividing surface is required. Another result of the theory is a model-free definition of the reaction coordinate quality (RCQ). The RCQ can be bounded from below by the directly computable observation quality (OQ), thus providing a measure allowing the RCQ to be optimized by tuning the experimental setup. Additionally, the respective partial probability distributions can be obtained for the reactant and product states along the observed order parameter, even when these strongly overlap. The effects of both filtering (averaging) and uncorrelated noise are also examined. The approach is demonstrated on numerical examples and experimental single-molecule force probe data of the p5ab RNA hairpin and the apo-myoglobin protein at low pH, here focusing on the case of two-state kinetics.

Keywords: rate theory; dividing surface; fitting correlation function; phenomenological rate; microscopic rate

The description of complex molecular motion through simple kinetic rate theories has been a central concern of statistical physics. A common approach, first-order rate theory, treats the relaxation kinetics among distinct regions of configuration space by single-exponential relaxation. There has been recent interest in estimating such rates from trajectories of single molecules, resulting from the recent maturation of measurement techniques able to collect extensive traces of single molecule extensions or fluorescence events [1, 2]. When the available observable is a good reaction coordinate in that it allows the slowly-converting states to be clearly separated (see Fig. 2I, left), classical rate theories apply and the robust estimation of transition rates is straightforward using a variety of means [3]. However, in the case in which the slowly-converting states overlap in the observed signal (see Fig. 2III, left), either due to the fact that the molecular order parameter used is a poorly separating them, or due to large noise of the measurement (see discussion in [4, 5]), a satisfactory theoretical description is missing and many estimators break down.

Most two-state rate theories and estimators are based on dividing the observed coordinate into a reactant and a product substate and then in some way counting transition events that cross the dividing surface. Transition state theory measures the instantaneous flux across this surface, which is known to overestimate the rate due to

the counting of unproductive recrossings over the dividing surface on short timescales [6].

Reactive flux theory [7] proposed to cope with this by counting a transition event only if it has succeeded to stay on the product side after a sufficiently long lag time τ . Reactive flux theory involves derivatives of autocorrelation functions that are numerically unreliable to evaluate [8]. In practice, one therefore typically estimates the relaxation rate *via* integration or performing an exponential fit to the tail of a suitable correlation function, such as the number correlation function of reactants or the autocorrelation function of the experimentally measured signal [3, 9, 10]. In order to split this relaxation rate into a forward and backward rate constant, a clear definition of the reactant and product substates is needed, which is difficult to achieve when these substates overlap in the observed signal.

Markov state models (MSMs) have recently become a popular approach to producing a simplified statistical model of complex molecular dynamics from molecular simulations.

While applicable only when the discretization of state space succeeds in separating the metastable conformations, these models can be regarded as steps towards a multistate rate theory. MSMs use a transition matrix describing the probability a system initially found in a substate i is found in substate j a lag time τ later. When the state division allows the metastable states of the system to be distinguished [11–14], the transition matrix with a sufficiently large choice of τ can be used to derive a phenomenological transition rate matrix that accurately describes the interstate dynamics [15]. This is explicitly done for the two-state case in [8]. It has been shown in [14, 16] that by increasing the number of substates used

* frank.no@fu-berlin.de (corresponding author)

[†] jan-hendrik.prinz@fu-berlin.de

[‡] chodera@mskcc.org

to partition state space, and hence using multiple dividing surfaces instead of a single one, these rate estimates become more precise. In the limit of infinitely many discretization substates, the eigenfunctions of the dynamical propagator in full phase space are exactly recovered, and the rate estimates become exact even for $\tau \rightarrow 0^+$ [17]. In practice, however, a finite choice of τ is necessary in order to have a small systematic estimation error, especially if “uninteresting” degrees of freedom such as momenta or solvent coordinates are discarded. An alternative way of estimating transition rates is by using a state definition that is incomplete and treats the transition region implicitly *via* committor functions that may better approximate the eigenfunctions of the dynamical propagator in this region [18–20].

The quality of the rate estimates in all of the above approaches relies on the ability to separate the slowly-converting states in terms of some dividing surface or state definition. These approaches often break down in practice when the available observables do not permit such a separation, i.e., when kinetically distinct states overlap in the histogram of the observed quantity. However, such a scenario may often arise in single-molecule experiments where the available order parameter depends on what is experimentally observable and may not necessarily be a good indicator of the slow kinetics. Moreover, consequences of the measurement process may increase the overlap between states, for example by bead diffusion in optical tweezer experiments or by shot noise in single-molecule fluorescence measurements. In favorable situations, the signal quality can be improved by binning the data to a coarser timescale (often simply referred to as “*filtering*”), thus reducing the fluctuations from fast processes and shot noise. However, the usefulness of such filtering is limited because the time window used needs to be much shorter than the timescales of interest — otherwise the kinetics will be distorted. In general, one has to deal with a situation where overlap between the slowly-converting states is present, both theoretically and practically.

Hidden Markov Models (HMMs) [21–23] and related likelihood methods [24] are able to estimate transition rates even in such situations, and have been recently successful in distinguishing overlapping states in molecules with complex kinetics [25, 26]. However, HMMs need a probability model of the measurement process to be defined, which can lead to biased estimates when this model is not adequate for the data analyzed. A recent approach, the signal pair-correlation analysis (PCA) [27] provides rate estimates without an explicit probability model, and instead requires the definition of indicator functions on which the measured signal can uniquely be assigned to one of the kinetically separated states. While this is often easier to achieve than finding an appropriate dividing surface, there is a trade-off between only using only data that is clearly resolved to be in one state or the other (thus minimizing the estimation bias), while avoiding discarding too much data (thus

minimizing the statistical error). Despite these slight limitations, both HMMs and PCA are practically very useful to identify and quantify hidden kinetics in the data. Yet, both are algorithmic approaches rather than a rate theory.

The recent success of single-molecule experiments and the desire for a robust rate estimation procedure that yields viable rate estimates even when highly overlapping states indicate clearly that the observed signal is a poor reaction coordinate highlights the need for a general and robust two-state rate theory for observed dynamics. Here, we make an attempt towards such a general rate theory for stochastic dynamics that are observed on a possibly poor reaction coordinate — often because the probed molecular order parameter is a poor choice, or because the measurement device creates overlap by noise-broadening the signal.

Our approach requires only mild assumptions to hold for the dynamics of the observed system: First, the dynamical law governing the time-evolution of the system *in its full phase space* — including all positions and velocities of the entire measured construct and the surround solvent — is assumed to be a time-stationary Markov process. We also require that the system obeys microscopic detailed balance in the full phase space, and supports a unique stationary distribution. These mild criteria are easily satisfied by a great number physical systems of interest in biophysics and chemistry.

When projected onto some measured observable, the dynamics of the system are no longer Markovian. In addition, the observed dynamics may be subjected to measurement noise. As a result, the resulting signal may not be easily separable into kinetically distinct states by a simple dividing surface, something that is often required for existing rate estimation procedures to work well.

Our framework allows us to (i) evaluate the quality of existing estimators and propose optimal estimators for the slowest relaxation rate, (ii) provide a model-free definition of the reaction coordinate quality (RCQ) and the observation quality (OQ) of the signal, and (iii) derive an optimal estimator for the transition rates between the slowly converting states, as well as their stationary probability densities, even if these strongly overlap in the observation.

The present rate theory is exclusively concerned with the systematic error in estimating rates and proposes “optimal” methods that minimize this systematic rate estimation error. Therefore all statements are strictly valid only in the data-rich regime. Explicit treatment of the statistical error in the data-poor regime is beyond the scope of the present work, but is briefly discussed at the end of the paper and in the supplementary information.

Full-space dynamics

We consider a dynamical system that follows a stationary and time-continuous Markov process \mathbf{x}_t in its full (and generally large and continuous) phase space Ω . \mathbf{x}_t is assumed to be ergodic with a unique stationary density $\mu(\mathbf{x})$. In order to be independent of specific dynamical models we use the general transition density $p_\tau(\mathbf{x}_t, \mathbf{x}_{t+\tau})$, i.e., the conditional probability density that given the system is at point $\mathbf{x}_t \in \Omega$ at time t , it will be found at point $\mathbf{x}_{t+\tau} \in \Omega$ a lag time τ later. We will at this point also assume that the dynamics obey microscopic detailed balance, i.e.,

$$\mu(\mathbf{x}_t) p_\tau(\mathbf{x}_t, \mathbf{x}_{t+\tau}) = \mu(\mathbf{x}_{t+\tau}) p_\tau(\mathbf{x}_{t+\tau}, \mathbf{x}_t), \quad (1)$$

which is true for systems that are not driven by external forces. In this case, $\mu(\mathbf{x})$ is a Boltzmann distribution in terms of the system's Hamiltonian. In some dynamical models, e.g. Langevin dynamics, Eq. 1 does not hold, but rather some generalized form of it [28]. In this case, the present theory also applies (see comment below), but in the interest of the simplicity of the equations, we will assume Eq. 1 subsequently.

For a two-state rate theory, we are interested in the slowest relaxation processes, and hence rewrite the transition density as a sum of relaxation processes (each associated with a different intrinsic rate) by expanding in terms of the eigenvalues λ_i and eigenfunctions ψ_i of the corresponding transfer operator [14, 16]:

$$p_\tau(\mathbf{x}_t, \mathbf{x}_{t+\tau}) = \sum_{i=1}^{\infty} e^{-\kappa_i \tau} \psi_i(\mathbf{x}_t) \mu(\mathbf{x}_{t+\tau}) \psi_i(\mathbf{x}_{t+\tau}). \quad (2)$$

Here,

$$\lambda_i(\tau) = e^{-\kappa_i \tau} \quad (3)$$

are eigenvalues of the propagator that decay exponentially with lag time τ . We order relaxation rates according to $\kappa_1 < \kappa_2 \leq \kappa_3 \leq \dots$ and thus $\lambda_1(\tau) > \lambda_2(\tau) \geq \lambda_3(\tau) \geq \dots$. The first term is special in that it is the only stationary process: $\kappa_1 = 0$, $\lambda_1(\tau) = 1$, $\psi_1(\mathbf{x}) = 1$, thus the first term of the sum is identical to $\mu(\mathbf{x})$. All other terms can be assigned a finite relaxation rate κ_i , or a corresponding relaxation timescale $t_i = \kappa_i^{-1}$, which are quantities of our interest. The eigenfunctions ψ_i are independent of τ and determine the structure of the relaxation process occurring with rate κ_i . The sign structure of $\psi_i(\mathbf{x})$ determines between which substates the corresponding relaxation process is switching and is thus useful for identifying metastable sets, i.e., sets of states that are long-lived and interconvert only by rare events [14, 29]. The eigenfunctions are chosen to obey the normalization conditions

$$\langle \psi_i, \psi_j \rangle_\mu = \int_{\Omega} d\mathbf{x} \psi_i(\mathbf{x}) \psi_j(\mathbf{x}) \mu(\mathbf{x}) = \delta_{ij} \quad (4)$$

and integration always runs over the full space of the integrated variable if not indicated otherwise. At a given

timescale τ of interest, fast processes with $\kappa \gg \tau^{-1}$ (and correspondingly $t_i \ll \tau$) will have effectively vanished and we are typically left with relatively few slowly-relaxing processes.

Finally, we define the μ -reweighted eigenfunctions,

$$\phi_i(\mathbf{x}) = \mu(\mathbf{x}) \psi_i(\mathbf{x}) \quad (5)$$

such that the normalization condition of eigenfunctions can be conveniently written as

$$\langle \phi_i, \phi_j \rangle = \int_{\Omega} d\mathbf{x} \phi_i(\mathbf{x}) \phi_j(\mathbf{x}) = \delta_{ij}. \quad (6)$$

Finally, the correlation density $c_\tau(\mathbf{x}_t, \mathbf{x}_{t+\tau})$, i.e., the joint probability density of finding the system at \mathbf{x}_t at time t and at $\mathbf{x}_{t+\tau}$ at time $t + \tau$ is related to the transition density p_t by

$$c_\tau(\mathbf{x}_t, \mathbf{x}_{t+\tau}) = \mu(\mathbf{x}_t) p_\tau(\mathbf{x}_t, \mathbf{x}_{t+\tau}). \quad (7)$$

Observed dynamics and two-state spectral rate theory

Let us consider the case that we are only interested in a single relaxation process — the slowest. Below, we sketch a rate theory for this case. Details of the derivation can be found in the supplementary information (SI). Based on the definitions above, the correlation density can then be written as:

$$\begin{aligned} c_\tau(\mathbf{x}_t, \mathbf{x}_{t+\tau}) &= \mu(\mathbf{x}_t) \mu(\mathbf{x}_{t+\tau}) \\ &\quad + e^{-\kappa_2 \tau} \mu(\mathbf{x}_t) \psi_2(\mathbf{x}_t) \mu(\mathbf{x}_{t+\tau}) \psi_2(\mathbf{x}_{t+\tau}) \\ &\quad + e^{-\kappa_3 \tau} \mu(\mathbf{x}_t) p_{\tau, \text{fast}}(\mathbf{x}_t, \mathbf{x}_{t+\tau}) \end{aligned} \quad (8)$$

where, if detailed balance (1) holds, the fast processes are given by Eq. (2):

$$p_{\tau, \text{fast}}(\mathbf{x}_t, \mathbf{x}_{t+\tau}) = \sum_{i=3}^{\infty} e^{-(\kappa_i - \kappa_3) \tau} \psi_i(\mathbf{x}_t) \mu(\mathbf{x}_{t+\tau}) \psi_i(\mathbf{x}_{t+\tau}) \quad (9)$$

If detailed balance does not hold on the full phase space, but rather some generalized form of it, the spectrum may have complex eigenvalues. Even in this case, the fast part of the dynamics can be bounded by $e^{-\kappa_3 \tau}$, and therefore Eq. (8) and the subsequent theory holds. See also discussion in [16].

Exact rate: κ_2 is often termed the *phenomenological rate*, as it governs the dominant relaxation rate of any observed signal in which the slowest relaxation process is apparent. The exact rate of interest κ_2 can be theoretically recovered as follows: If we know the exact corresponding eigenfunction $\psi_2(\mathbf{x})$, it follows from Eq. (2) and (4) that its autocorrelation function evaluates to:

$$\begin{aligned} \lambda_2(\tau) &= \langle \psi_2(\mathbf{x}_t) \psi_2(\mathbf{x}_{t+\tau}) \rangle_t \\ &= \int_{\Omega} d\mathbf{x}_t \int_{\Omega} d\mathbf{x}_{t+\tau} c_\tau(\mathbf{x}_t, \mathbf{x}_{t+\tau}) \psi_2(\mathbf{x}_t) \psi_2(\mathbf{x}_{t+\tau}) \\ &= e^{-\kappa_2 \tau} \end{aligned} \quad (10)$$

where $\langle \cdot \rangle_t$ denotes the time average, that is here identical to the ensemble average due to ergodicity of the dynamics.

The correlation function $\langle \psi_2(0)\psi_2(\tau) \rangle_t$ yields the exact eigenvalue $\lambda_2(\tau)$ and thus also an exact rate estimate $\hat{\kappa}_2 = -\tau^{-1} \ln \lambda_2(\tau) = \kappa_2$, independently of the choice of τ .

Projected dynamics without measurement noise: Suppose we observe the dynamics of an order parameter $y \in \mathbb{R}$ that is a function of the configuration \mathbf{x} . Examples are the distance between two groups of the molecule, or a more complex observable such as the Förster resonance transfer efficiency associated to a given configuration. See Fig. 1 for an illustration. We first assume that no additional measurement noise is present. The analysis of a molecular dynamics simulation where a given order parameter is monitored is one example of such a scenario. Now, it is no longer possible to compute the rate via Eq. (10) or some direct approximation of Eq. (10), since the full configuration space Ω in which the eigenfunction ψ_2 exists can no longer be recovered once the dynamics has been projected onto an order parameter. Instead, we are forced to work with functions of the observable y . While the theory is valid for multidimensional observables y , the equations below assume $y \in \mathbb{R}$ for simplicity.

We have two options for deriving the relevant rate equations for the present scenario: As a first option, we note that a projection that is free of noise can be regarded as a function $y(\mathbf{x}) : \Omega \rightarrow \mathbb{R}$. Thus, any function $\psi_2(y)$ of elements in observable space \mathbb{R} that aims at approximating the dominant eigenfunction ψ_2 , can be also regarded as a function in full space Ω via $\tilde{\psi}_2(y) = \psi_2(y(\mathbf{x}))$. When following this idea, one can use the variational principle of conformation dynamics [30] (see also the discrete-state treatment in [20]), in order to derive the rate equations for the observed space dynamics. See SI for details.

However, since we aim to include the possibility of measurement noise in a second step, we derive a more general approach (see SI), which is summarized subsequently. Consider the function $\chi_p(y | \mathbf{x})$ that denotes the output probability density with which each configuration of the full state space, $\mathbf{x} \in \Omega$, yields a measured value $y \in \mathbb{R}$. In the case of simply projecting \mathbf{x} -values without noise to specific y -values, χ has the simple form:

$$\chi_p(y' | \mathbf{x}) = \delta(y' - y(\mathbf{x})) \quad (11)$$

This allows the correlation density in the observable space to be written as:

$$\begin{aligned} & c_\tau(y_0, y_\tau) \\ &= \int_{\Omega} d\mathbf{x}_0 \int_{\Omega} d\mathbf{x}_\tau \chi_p(y_0 | \mathbf{x}_0) c_\tau(\mathbf{x}_0, \mathbf{x}_\tau) \chi_p(y_\tau | \mathbf{x}_\tau) \\ &= \mu^y(y_0) \mu^y(y_\tau) + \sum_{i=2}^{\infty} \lambda_i(\tau) \phi_i^y(y_0) \phi_i^y(y_\tau) \end{aligned} \quad (12)$$

where we have used superscript y to indicate the projection of a full configuration space function onto the or-

der parameter: $\mu^y(y)$ is the observed stationary density that can be estimated from a sufficiently long simulation by histogramming the values of y . Mathematically, it is given by:

$$\mu^y(y) = \int_{\Omega} d\mathbf{x} \chi_p(y | \mathbf{x}) \mu(\mathbf{x}) \quad (13)$$

ϕ_i^y are the projected eigenfunctions:

$$\phi_i^y(y) = \int_{\Omega} d\mathbf{x} \chi_p(y | \mathbf{x}) \phi_i(\mathbf{x}) \quad (14)$$

In order to arrive at an expression of the rate κ_2 , we propose a trial function in observation space, $\tilde{\psi}_2(y)$, which we require to be normalized by

$$\langle \tilde{\psi}_2, 1 \rangle_{\mu^y} = 0, \quad \langle \tilde{\psi}_2, \tilde{\psi}_2 \rangle_{\mu^y} = 1, \quad (15)$$

and evaluate its autocorrelation function as:

$$\begin{aligned} \langle \tilde{\psi}_2(y_0) \tilde{\psi}_2(y_\tau) \rangle &= \int_{\mathbb{R}} dy_0 \int_{\mathbb{R}} dy_\tau \tilde{\psi}_2(y_0) c_\tau(y_0, y_\tau) \tilde{\psi}_2(y_\tau) \\ &= \alpha_y e^{-\kappa_2 \tau} + \sum_{i>2} \langle \tilde{\psi}_2, \phi_i^y \rangle^2 e^{-\kappa_i \tau} \end{aligned} \quad (16)$$

where

$$\alpha_y = \langle \tilde{\psi}_2, \phi_2^y \rangle^2. \quad (17)$$

In contrast to Eq. (10), both $\tilde{\psi}_2$ and ϕ_i^y live on the observable space \mathbb{R} . In the special case that $\psi_2(\mathbf{x})$ is constant in all other variables than $y(\mathbf{x})$, the projection is lossless ($\phi_2^y(y(\mathbf{x})) = \psi_2(\mathbf{x})$ and $\psi_2^y(y(\mathbf{x})) = \psi_2(\mathbf{x})$ for all \mathbf{x}), and using the choice $\tilde{\psi}_2 = \psi_2^y$, we recover $\langle \tilde{\psi}_2, \phi_2^y \rangle = \langle \psi_2, \phi_2 \rangle = 1$, and thus the exact rate estimate via Eq. (10). In general, however, the eigenfunction $\psi_2(\mathbf{x})$ does vary in other variables than y , and therefore $\tilde{\psi}_2$ can at best approximate the full-space eigenfunction via $\tilde{\psi}_2(y(\mathbf{x})) \approx \psi_2(\mathbf{x})$.

Observed dynamics with measurement noise: Suppose that an experiment is conducted in which each actual order parameter value $y(\mathbf{x}) \in \mathbb{R}$ is measured with additional noise, yielding the observed value $o \in \mathbb{R}$. In time-binned single-molecule fluorescence experiments such noise may come from photon counting shot noise for a given binning size. In optical tweezer experiments such noise may come from bead diffusion and handle elasticity, assuming that bead and handle dynamics are faster than the kinetics of the molecule of interest. See Fig. 1 for an illustration. Note that we only treat the situation of uncorrelated noise. In situations where the experimental configuration changes the kinetics, e.g., when the optical bead diffusion is slow, thus exhibiting different transition rates than the isolated molecule, our analysis always reports the rate of the overall observed system. The task of correcting the measured rates so as to estimate the rates of the pure molecule is beyond the scope of this work and can, for example, be attempted via dynamical deconvolution [31, 32] or other approaches [33].

Like before, the probability of observing a measurement value $o \in \mathbb{R}$ given that the true configuration was $\mathbf{x} \in \Omega$ can be given by an output probability:

$$\chi_{pd}(o | \mathbf{x}) = \int_{\mathbb{R}} dy \chi_d(o | y) \chi_p(y | \mathbf{x}), \quad (18)$$

which convolves the projection from \mathbf{x} to the value of the order parameter, $\chi_p(y | \mathbf{x})$, with the subsequent dispersion of the signal by noise, $\chi_d(o | y)$. Despite the fact that dispersion operates by a different physical process than projection, the same analysis as above applies. We define the projected and dispersed stationary density and eigenfunctions:

$$\begin{aligned} \mu^o(o) &= \int_{\Omega} d\mathbf{x} \chi_{pd}(o | \mathbf{x}) \mu(\mathbf{x}) \\ &= \int_{\mathbb{R}} dy \chi_d(o | y) \mu^y(y) \end{aligned} \quad (19)$$

$$\begin{aligned} \phi_i^o(o) &= \int_{\Omega} d\mathbf{x} \chi_{pd}(o | \mathbf{x}) \phi_i(\mathbf{x}) \\ &= \int_{\mathbb{R}} dy \chi_d(o | y) \phi_i^y(y) \end{aligned} \quad (20)$$

which are “smeared out” by noise compared to the purely projected density and eigenfunctions ϕ_i^y . As above, the autocorrelation function of a probe function $\tilde{\psi}_2(o)$ is given by:

$$\langle \tilde{\psi}_2(o_0) \tilde{\psi}_2(o_\tau) \rangle = \alpha_o e^{-\kappa_2 \tau} + \sum_{i \geq 2} \langle \tilde{\psi}_2, \phi_i^o \rangle^2 e^{-\kappa_i \tau} \quad (21)$$

with

$$\alpha_o = \langle \tilde{\psi}_2, \phi_1^o \rangle^2. \quad (22)$$

The observation process including noise is a more general process than the observation process excluding noise, therefore — unless the distinction is important — we will generally refer to the observation as o subsequently, whether noise is included in the observation or not.

Filtered dynamics: The effect of measurement noise may be reduced by filtering (averaging) the observed signal $o(t) \rightarrow \bar{o}(t)$, for example by averaging the signal value over a time window of length W . Note that this operation will introduce memory of length W into the signal and will impair the estimation of all rates which are close to W^{-1} . Fig. 1 of the SI illustrates the effect of filtering on the estimation quality of rates in a simple example. To make sure that the filter used does not impair the rate estimates, we recommend that the filter length be at least a factor of 10 smaller than the timescales of interest, $t_2 = \kappa_2^{-1}$. The filtered signal $\bar{o}(t)$ can then be used as input to the various rate estimators discussed in this paper, but the theory of systematic errors given in the subsequent section may no longer apply because filtering destroys the Markovianity of the original dynamic process in the full state space. A more extensive treatment of filtering is given in the SI.

Direct rate estimate: In all of the above cases, the autocorrelation function of the trial function $\tilde{\psi}_2$ does not yield the exact eigenvalue $\lambda_2(\tau)$, but some approximation $\tilde{\lambda}_2(\tau)$. For $\tau \gg \kappa_3^{-1}$, which can readily be achieved for clear two-state processes where a time scale separation exists ($\kappa_2 \gg \kappa_3$), the terms involving the fast processes disappear:

$$\tilde{\lambda}_2(\tau) \approx \alpha_o e^{-\kappa_2 \tau}. \quad (23)$$

This suggests that the true rate κ_2 , as well as the prefactor α_o that may serve as a basis to measure the observation quality, could be recovered from large τ decay of an appropriately good trial function even from the observed signal. We elaborate this concept in subsequent sections. Note that in experiments the relaxation rates κ_2, κ_3 , etc, are initially unknown and hence the validity of Eq. (23) can only be checked a posteriori, e.g., by the fact that estimates based upon Eq. (23) are independent of the lag time τ .

Existing rate estimators

Many commonly used rate estimators consist of two steps: (1) they (explicitly or implicitly) calculate an autocorrelation function $\tilde{\lambda}_2(\tau)$ of some function $\tilde{\psi}_2$, and (2) transform $\tilde{\lambda}_2(\tau)$ into a rate estimate $\tilde{\kappa}_2$. In order to derive an optimal estimator, it is important to understand how the systematic error of the estimated rate depends on each of the two steps. Therefore, we now rephrase existing rate estimators in the formalism of spectral rate theory. The SI contains a detailed derivation of the subsequent results.

Many rate estimators operate by defining a single dividing surface which splits the state space into reactants A and products B . Calling $h_A(o)$ the indicator function which is 1 for set A and 0 for set B , one may define the normalized fluctuation autocorrelation function of state A [34]

$$\tilde{\lambda}_2(t) = \frac{\langle h_A(0) h_A(\tau) \rangle - \langle h_A \rangle^2}{\langle h_A^2 \rangle - \langle h_A \rangle^2} = \langle \tilde{\psi}_2(0) \tilde{\psi}_2(\tau) \rangle \quad (24)$$

that can also be interpreted as an autocorrelation function $\tilde{\lambda}_2(t)$ with a step function $\tilde{\psi}_{2,\text{divide}}(o) = (h_A(o) - \pi_A) / \sqrt{\pi_A \pi_B}$. Here, $\pi_A = \langle h_A \rangle_\mu$ is the stationary probability of state A and $\pi_B = 1 - \pi_A$ the stationary probability of state B . Other rate estimates choose $\tilde{\psi}_2$ to be the signal $o(t)$ itself or the committor function between two pre-defined subsets of the o coordinate [19]. We show that none of these choices is optimal, and the optimal choice of $\tilde{\psi}_2$ will be derived in the subsequent section.

Existing rate estimators largely differ by step (2), i.e., how they transform $\tilde{\lambda}_2(t)$ into a rate estimate $\tilde{\kappa}_2$. This procedure then determines the functional form of the systematic estimation error. We subsequently list bounds for these errors (see SI for derivation). The

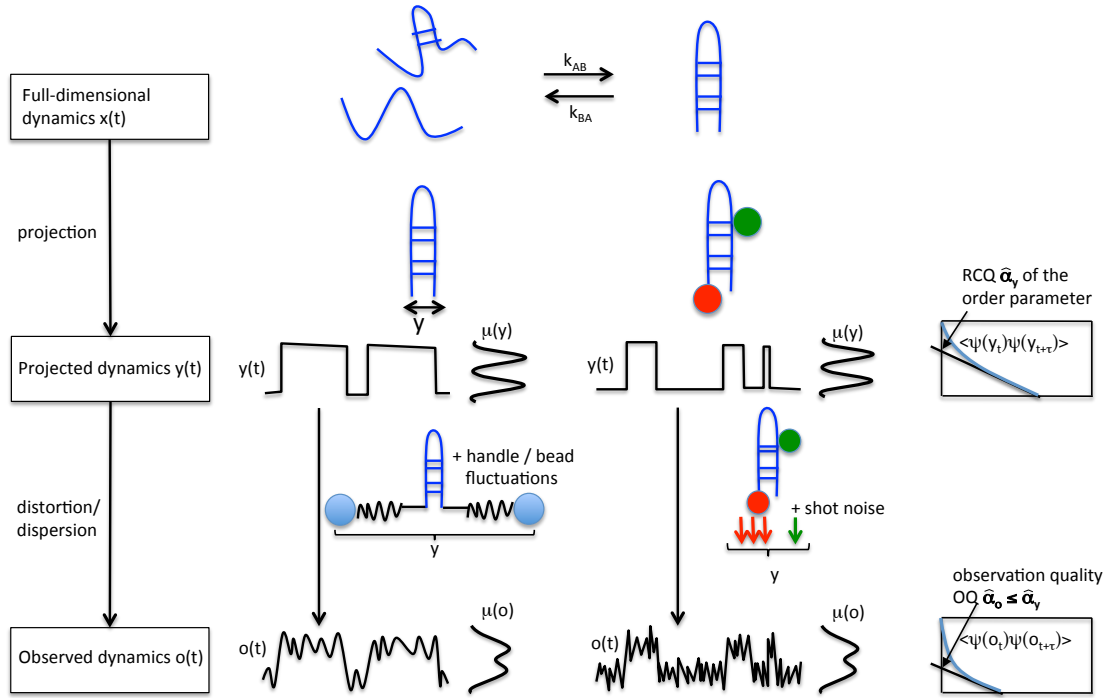


Figure 1. **Illustration of the observed dynamics for which a rate theory is formulated here.** *Top row:* the full-dimensional dynamics $\mathbf{x}(t)$ in phase space Ω . These dynamics are assumed to be Markovian, ergodic, and reversible as often found for physical systems in thermal equilibrium. Furthermore, the theory here is formulated for two-state kinetics, i.e., the system has two metastable states exchanging at rates k_{AB} and k_{BA} , giving rise to a relaxation rate of $\kappa_2 = k_{AB} + k_{BA}$. *Middle row:* One order parameter $y(\mathbf{x})$ of the system is observed, such as a distance between two groups of a molecule, or the FRET efficiency between two fluorescent groups. The projection of the full-space dynamics $\mathbf{x}(t)$ onto the order parameter y generates a time series $y(t)$, that may, however not be directly observable. The projection also acts on functions of state space, such as the stationary distribution of configurations in full state space that is projected onto a density in the observable, $\mu(y)$. The reaction coordinate quality $\hat{\alpha}_y$ measures how well the order parameter y resolves the slow transition. It is 1 when A and B are perfectly separated and 0 when they completely overlap. *Bottom row:* the experimental device used may distort or disperse the signal, for example by adding noise. The resulting observed signal $o(t)$ is distorted and the observable density $\mu^o(o)$ is smoothed. $\hat{\alpha}_o$ measures the observation quality (OQ) of the observed signal and it is shown in the SI that $\hat{\alpha}_o \leq \hat{\alpha}_y$ holds.

prefactor α in the equations below either refers to α_p (purely projected dynamics) or α_o (dynamics with noise), whichever is appropriate.

Reactive flux rate. Chandler, Montgomery and Berne [7, 35] considered the reactive flux correlation function as a rate estimator: $\tilde{\kappa}_{2,\text{rf}}(\tau) = -\frac{d}{dt}\tilde{\lambda}_2(\tau)$. Its error is

$$\tilde{\kappa}_{2,\text{rf}} - \kappa_2 = \kappa_2(\alpha - 1) + \sum_{i>2} \langle \tilde{\psi}_2, \psi_i \rangle_{\mu}^2 \kappa_2 e^{-\kappa_i \tau} > 0 \quad (25)$$

which becomes 0 for the perfect choice of $\tilde{\psi}_2 = \psi_2$ that leads to $\alpha = 1$, but can be very large otherwise.

Transition state theory rate. The transition state theory rate, which measures the instantaneous flux across the dividing surface between A and B , is often estimated by the trajectory length divided by the number of crossings of the dividing surface. Its simplicity makes it a widely popular choice for practical use in experiments and theory (despite its tendency to produce biased estimates, as we will discuss later).

In order to arrive at an expression for the estimation error, the TST rate can be expressed as the short-time limit of the reactive flux [7], $\tilde{\kappa}_{2,\text{tst}} = \lim_{\tau \rightarrow 0^+} \tilde{\kappa}_{2,\text{rf}}(\tau)$ such that the error in the rate is given by

$$\tilde{\kappa}_{2,\text{tst}} - \kappa_2 = \kappa_2(\alpha - 1) + \sum_{i>2} \langle \tilde{\psi}_2, \psi_i \rangle_{\mu}^2 \kappa_2 > \tilde{\kappa}_{2,\text{rf}} - \kappa_2 \quad (26)$$

which is always an overestimate of the true rate and of the reactive flux rate.

Integrating the correlation function. Another means of estimating the rate is via the integral of the correlation function, $\tilde{\kappa}_{2,\text{int}} = -(\int_0^\infty d\tau \tilde{\lambda}_2(\tau))^{-1}$ (see, e.g., Eq. 3.6 of [7]), with the error:

$$\tilde{\kappa}_{2,\text{int}} - \kappa_2 = \kappa_2 \left(\frac{1 - \alpha + \sum_{i>2} \langle \psi_i, \tilde{\psi}_2 \rangle_{\mu}^2 \frac{\kappa_2}{\kappa_i}}{\alpha + \sum_{i>2} \langle \psi_i, \tilde{\psi}_2 \rangle_{\mu}^2 \frac{\kappa_2}{\kappa_i}} \right) \quad (27)$$

in the special case that $\kappa_3 \gg \kappa_2$ (time scale separation), the error is approximately given by $\kappa_2(1 - \alpha)/\alpha$. Thus,

the error of this estimator becomes zero for $\alpha = 1$, which is only the case for a reaction coordinate with no noise, and no further projection (e.g. by using a dividing surface). The error may be very large in other cases ($\alpha < 1$).

Single- τ rate estimators: A simple rate estimator takes the value of the autocorrelation function of some function $\tilde{\psi}_2$ at a single value of τ , and transforms it into a rate estimate by virtue of Eq. (23).

We call these estimators *single- τ estimators*. Ignoring statistical uncertainties, they yield a rate estimate of the form

$$\tilde{\kappa}_{2,\text{single}} = -\frac{\ln \tilde{\lambda}_2(\tau)}{\tau} \quad (28)$$

Quantitatively, the error can be bounded by the expression (see derivation in the SI):

$$\tilde{\kappa}_{2,\text{single}} - \kappa_2 \leq -\frac{\ln \alpha}{\tau}. \quad (29)$$

The error becomes identical to this bound for systems with a strong timescale separation, $\kappa_3 \gg \kappa_2$. Eq. (29) decays relatively slowly in time (with τ^{-1} . See Fig. 2 for a two-state example). It will be shown below that methods that estimate rates from counting the number of transitions across a dividing surface, such as Markov state models (MSMs), are single- τ estimators and are thus subject to the error given by Eq. (29).

The systematic error of single- τ estimators results from the fact that Eq. (28) effectively attempts to fit the tail of a multi-exponential decay $\tilde{\lambda}_2(\tau)$ by a single-exponential with the constraint $\tilde{\lambda}_2(0) = 1$. Unfortunately, the ability to improve these estimators by simply increasing τ is limited because the statistical uncertainty of estimating Eq. 23 quickly grows with increasing τ [36].

Multi- τ rate estimators: To avoid the error given by Eq. (29), it is advisable to estimate the rate by evaluating the autocorrelation function $\tilde{\lambda}_2(\tau)$ at multiple values of τ . This can be done e.g., by performing an exponential fit to the *tail* of the $\tilde{\lambda}_2(\tau)$, thus avoiding the constraint $\tilde{\lambda}_2(0) = 1$ [3, 10]. The corresponding estimation error $\hat{\kappa}_{2,\text{mult}} - \kappa_2$ is bounded by:

$$\hat{\kappa}_{2,\text{mult}} - \kappa_2 < c \frac{1 - \alpha}{\alpha} e^{-\tau_1(\kappa_3 - \kappa_2)} \quad (30)$$

where τ_1 is the first lag time from the series (τ_1, \dots, τ_m) used for fitting, and the constant c also depends on the lag times and the fitting algorithm used. The SI shows that for several fitting algorithms, such as a least-squares procedure at the time points $(\tau, 2\tau, \dots, m\tau)$, c is such that

$$\hat{\kappa}_{2,\text{mult}} \leq \tilde{\kappa}_{2,\text{single}}. \quad (31)$$

Thus, the multi- τ estimator is always better than the single- τ estimator (see SI). The main advantage of multi- τ estimators is that their convergence rate is exponential

in τ when the time scale separation $\kappa_3 - \kappa_2$ is not vanishing (compare to Eq. 29). Thus, multi- τ estimators are better when the timescale separation between the slowest and the other relaxation rates in the system is larger.

In the absence of statistical error, all of the above rate estimation methods are seen to yield an overestimation of the rate, $\tilde{\kappa}_2 \geq \kappa_2$.

Optimal choice of $\tilde{\psi}_2$

It was shown above that multi- τ estimators are the best choice for converting an autocorrelation function into a rate estimate. However, what is the best possible choice $\hat{\psi}_2 = \tilde{\psi}_{2,\text{optimal}}$ given a specific observed time series o_t ? In other words, which function should the observed dynamics be projected upon in order to obtain an optimal rate estimator? Following Eq. (29), the optimal choice $\hat{\psi}_2$ is the one which maximizes the parameter α , as this will minimize the systematic error from a direct rate estimation by virtue of Eq. (29), and also minimize the systematic error involved in estimating κ_2 from an exponential fit to Eq. (23). We are thus seeking the solution of:

$$\hat{\psi}_2 = \arg \max_{\tilde{\psi}_2} \alpha = \arg \max_{\tilde{\psi}_2} \tilde{\lambda}_2(\tau) \quad (32)$$

for some $\tau > 0$, subject to the normalization Eq. (15). Here, $\arg \max_{\tilde{\psi}_2} \alpha$ denotes the function that maximizes α over the space of functions $\tilde{\psi}_2(o)$. If the system has two-state kinetics, i.e., only $\psi_1(\mathbf{x}) = 1$ and $\psi_2(\mathbf{x})$ are present as dominant eigenfunctions, the problem (32) is solved by the projected eigenfunction:

$$\hat{\psi}_2 = \psi_2^o \quad (33)$$

How can the best possible $\hat{\psi}_2$ be determined from the observed time series? For a sufficiently large set of n basis functions, $\gamma = \{\gamma_1(o), \dots, \gamma_n(o)\}$, the optimal eigenfunction $\hat{\psi}_2$ is approximated by a linear combination $\hat{\psi}_2(o) \approx \sum_{i=1}^n c_i \gamma_i(o)$ with coefficients $\mathbf{c} = \{c_1, \dots, c_n\}$. When γ is chosen to be an orthogonal basis set, then $\hat{\psi}_2 = \arg \max_{\tilde{\psi}_2} \alpha$ can be approximated by the Ritz method [30, 37]. An easy way to do this approximation in practice is to perform a fine discretization of the observable o by histogram windows. Using a binning with bin boundaries b_1, \dots, b_{n+1} , and the corresponding indicator functions

$$\gamma_i(o) = \begin{cases} 1 & \text{if } i \in [b_i, b_{i+1}) \\ 0 & \text{else} \end{cases}, \quad (34)$$

then the above optimization problem is solved by estimating the transition probability matrix with elements

$$T_{ij} = \mathbb{P}(o(\tau) \in [b_j, b_{j+1}) \mid o(0) \in [b_i, b_{i+1})) \quad (35)$$

and calculating \mathbf{c} as the second eigenvector:

$$\mathbf{T}\mathbf{c} = \lambda_2 \mathbf{c} \quad (36)$$

where $\lambda_2 < 1$ is the second-largest eigenvalue of \mathbf{T} . If the system has two-state kinetics, i.e., only $\psi_1(\mathbf{x}) = 1$ and $\psi_2(\mathbf{x})$ are present as dominant eigenfunctions, the estimate $\hat{\psi}_2$ is independent of the choice of τ in Eq. (35). Thus, in real systems, τ should be chosen to be at least a multiple of κ_3^{-1} (e.g., $\tau \geq 3\kappa_3^{-1}$, as indicated by a constant rate κ_2 estimate using a multi- τ estimator (Eq. (30)). Note that a given optimal $\hat{\psi}_2(o)$ can still be used with single- τ and multi- τ rate estimators that would produce different estimates for κ_2 .

Note that $\hat{\psi}_2$ according to the procedure described here is only optimal for the case when the observed signal is obtained by projecting the high-dimensional data onto the observable, but is no longer optimal in the presence of noise, and especially large noise. In order to choose $\hat{\psi}_2$ optimal when noise is present, a generalized Hermitian eigenvalue problem must be solved instead of Eq. (36) which includes a mixing matrix whose elements quantify how much the observable bins are mixed due to measurement noise. Since this approach is not very straightforward and in most practical cases only leads to small improvements, we do not pursue this approach further here. We rather note that it is often practical to reduce the noise level by carefully filtering the recorded data, provided that the filter length is much shorter than the timescales of interest.

Reaction coordinate quality (RCQ), estimation quality, and observation quality (OQ)

Evaluating the suitability of a given observable for capturing the slow kinetics is of great general interest. Although there is not a unique way of quantifying this suitability of the observable, the term reaction coordinate quality (RCQ) is often used. Previous studies have proposed ways to measure the RCQ that are based on comparing the observed dynamics to specific dynamical models or testing the ability of the observable to model the committor or splitting probability between two chosen end-states A and B [4, 5, 38]. These metrics are either only valid for specific models of dynamics or themselves require a sufficiently good separation of A and B by definition, restricting their applicability to observables with rather good RCQs.

The prefactor $\hat{\alpha}_y$ (see also Fig. 1) is a measure between 0 and 1, quantifying the relative amplitude of the slowest relaxation in the autocorrelation function after projection of the full-space dynamics onto the molecular observable employed. The value $\hat{\alpha}_y$ only depends on the observable itself, and is free of modeling choices and of the way rates are estimated from the signal. Therefore, we propose that α_y is the reaction coordinate quality (RCQ).

However, α_y is not directly measurable: for a given observation, both the projection of the full-space dynamics and measurement noise compromise the quality of the signal, and these effects cannot be easily sep-

arated. In addition, the actual pre-factor that is obtained in a given estimate of the signal autocorrelation function, α_o depends on the way the data is analyzed, namely the functional form $\tilde{\psi}_2(o)$ used to compute the autocorrelation function $\tilde{\lambda}_2(\tau)$. Therefore, α_o is just an estimation quality.

Fortunately, the ambiguity of the estimation quality is removed for the optimal choice $\tilde{\psi}_2 = \hat{\psi}_2$ (Eq. (32)), which maximizes α_o . In this case we denote this prefactor $\hat{\alpha}_o$, where $\hat{\alpha}_o = \alpha_o(\hat{\psi}_2) \geq \alpha_o(\tilde{\psi}_2)$. Since $\hat{\alpha}_o$ only depends on the observed signal, and not on the way of analyzing it, we term it observation quality (OQ). The OQ is a very important quantity, because by virtue of Eqs. (29) and (30), $\hat{\alpha}_o$ quantifies how large the error in our rate estimate can be for the optimal choice $\tilde{\psi}_2 = \hat{\psi}_2$.

Our definitions of RCQ and OQ are very general, as they makes no assumptions about the class of dynamics in the observed coordinate, and does not depend on any subjective choices such as the choice of two reaction end-states A and B in terms of the observable o . Through the derivation above it has also been shown that $\hat{\alpha}_o$ measures the fraction of amplitude by which the slowest process is observable, which is exactly the property one would expect from a measure of the RCQ: $\hat{\alpha}_o$ is 1 for a perfect reaction coordinate with no noise, and 0 if the slowest process is exactly orthogonal to the observable, or has been completely obfuscated by noise.

While the OQ is the quantity that can be computed from the signal, an analyst is typically interested in the RCQ $\hat{\alpha}_y$ that is due to the choice of the molecular order parameter. Unless a quantitative model of the dispersion function $\chi_d(o | y)$ is known, the RCQ $\hat{\alpha}_y$ before adding noise cannot be recovered. (see also Fig. 1 for an illustration). However, we can still quantitatively relate $\hat{\alpha}_y$ and $\hat{\alpha}_o$, and thereby show that even the OQ is very useful. For this, we derive a theory of observation quality. While the detailed derivation is found in the SI, we just summarize the most important results here:

1. When observing the order parameter y without noise and projecting the observation onto the optimal indicator function $\tilde{\psi}_2 = \hat{\psi}_2^o$, the RCQ can be expressed as the weighted norm of the projected eigenfunction, expressed by the scalar product:

$$\hat{\alpha}_y = \langle \phi_2^y, \psi_2^y \rangle \quad (37)$$

2. Unless the projection perfectly preserves the structure of the full-space eigenfunction ψ_2 , we have $\hat{\alpha}_y < 1$. Thus, almost every observable reduces the RCQ.
3. When additional noise is present, the OQ can be expressed as the weighted norm of the projected and noise-distorted eigenfunction:

$$\hat{\alpha}_o = \langle \phi_2^o, \psi_2^o \rangle \quad (38)$$

4. The RCQ $\hat{\alpha}_y$ due to the projection onto the selected molecular order parameter alone, and the OQ $\hat{\alpha}_o$

including measurement noise are related by:

$$\hat{\alpha}_o \leq \hat{\alpha}_y, \quad (39)$$

i.e., adding noise means that the OQ is smaller than the RCQ.

The inequality (39) implies that we can use the OQ $\hat{\alpha}_o$ in order to both optimize the experimental setup and the order parameter used. For example in an optical tweezer measurement, we can change laser power and handle length so as to maximize $\hat{\alpha}_o$, thus making $\hat{\alpha}_o$ and $\hat{\alpha}_y$ more similar and reducing the effect of noise on the measurement quality. On the other hand, since $\hat{\alpha}_o$ is a lower bound for $\hat{\alpha}_y$, we can also use it ensure a minimal projection quality: When the measurement setup itself is kept constant we can compare the measurements of different constructs (e.g., different FRET labeling positions or different attachment sites in a tweezer experiment). The best value $\hat{\alpha}_o$ corresponds to the provably best construct.

Finally, $\hat{\alpha}_o$ can be determined by fitting the autocorrelation function of $\hat{\psi}_2$, as described in the spectral estimation procedure described below. Figs. 2-5 show estimates of the OQ of different observed dynamics (via spectral estimation) and of the estimation quality using other rate estimators.

Markov (state) models (MSMs)

MSMs have recently gained popularity in the modeling of stochastic dynamics from molecular simulations [12, 14, 15, 39, 40]. MSMs can be understood as a way of implicitly performing rate estimates via discretizing state space into small substates. Let us consider a MSM obtained by finely discretizing the observed space y into bins and estimating a transition matrix $\mathbf{T}(\tau)$ amongst these bins. We have seen that this procedure approximately solves the optimization problem of Eq. (32) and the leading eigenvector of $\mathbf{T}(\tau)$ approximates the projection of the true second eigenfunction, $\hat{\psi}_2^o(o)$, available for the given observable o . Ref. [15] has suggested to use the implied timescale $\hat{t}_2 = -\tau / \ln(\hat{\lambda}_2(\tau))$ as an estimate for the system's slowest relaxation timescale, and at the same time for a test which choice of τ leads to a MSM with a small approximation error. These implied timescales correspond to the inverse relaxation rates and therefore the MSM rate estimate is described by Eq. (28) with the choice $\tilde{\psi}_2 = \hat{\psi}_2$. A sufficiently fine MSM thus serves as an optimal single- τ rate estimator as its estimation quality approaches the true OQ $\hat{\alpha}_o$ for the observed signal that is being discretized. However, when this signal has a poor OQ $\hat{\alpha}_o$ since it is poorly separating the slowly-converting states, there is a substantial rate estimator error according to Eq. (29) that decays slowly with τ^{-1} . This likely explains the slow convergence of implied timescales shown in recent MSM simulation studies [12–15, 41].

Estimating state densities and microscopic transition rates

When the rate κ_2 is exactly known, the microscopic transition rates between the two interchanging states, k_{AB} and k_{BA} could be calculated from the equations:

$$\pi_A k_{AB} = \pi_B k_{BA}, \quad (40)$$

$$k_{AB} + k_{BA} = \kappa_2 \quad (41)$$

where π_A and π_B are the stationary probabilities of states A and B :

$$\pi_A = \int_o do \mu_A^o(o) \quad (42)$$

$$\pi_B = \int_o do \mu_B^o(o) = 1 - \pi_A \quad (43)$$

with $\mu_A^o(o)$ and $\mu_B^o(o)$ being the partial densities of states A and B in the observable o , respectively.

Here we attempt to estimate both the partial densities, $\mu_A^o(o)$ and $\mu_B^o(o)$, and from these the microscopic transition rates via Eqs. (40) and (41). The difficulty is that $\mu_A^o(o)$ and $\mu_B^o(o)$ can significantly overlap in o , both due to the way the order parameter used projects the molecular configurations onto the observable, and due to noise broadening of the measurement device. This reveals a fundamental weakness of dividing-surface approaches. Although a dividing surface estimator can estimate the rate κ_2 for sufficiently large τ without bias via Eq. (30), it cannot distinguish between substates on one side of the barrier, and thus assumes the partial densities $\mu_A^o(o)$ and $\mu_B^o(o)$ to be given by cutting the full density $\mu^o(o)$ at the dividing surface. When the true partial densities overlap, this estimate can be far off (compare the curves in Fig. 2II panel 5, and Fig. 2III panel 5). Consequently, incorrect estimates for the microscopic rates k_{AB} and k_{BA} are obtained when Eqs. (40) and (41) are used with π_A and π_B that are simply the total densities “left” and “right” of the dividing surface.

Hidden Markov models approach this problem by proposing a specific functional form of $\mu_A^o(o)$ and $\mu_B^o(o)$, for example a Gaussian distribution, and then estimating the parameters of this distribution with an optimization algorithm [21, 23]. This approach is very powerful when the true functional form of the partial densities is known, but will give biased estimates when the wrong functional form is used.

Here, we propose a nonparametric solution that can estimate the form of the partial densities μ_A^o and μ_B^o , and the microscopic transition rates \hat{k}_{AB} and \hat{k}_{BA} in most cases without bias. For this, we employ the theory of Perron cluster cluster analysis (PCCA+) [17, 42] which is based on PCCA theory [29, 43] which allows for a way of splitting state space into substates and at the same time maintain optimal approximations to the exact eigenfunctions (here ψ_2): The state assignment must be fuzzy, i.e., instead of choosing a dividing surface that uniquely assigns points o to either A or B , we have fuzzy

membership functions $\chi_A(o)$ and $\chi_B(o)$ with the property $\chi_A(o) + \chi_B(o) = 1$. These membership functions can be calculated after ψ_2 is known.

In order to compute the membership χ_A and χ_B , the memberships of two points of the observable o must be fixed. The simplest choice is to propose two observable values that are pure, i.e., that have a membership of 1 to A and B each. Such an approach is also proposed by the signal-pair correlation analysis approach [27] where the pure values need to be defined by the user. However at this point of our analysis, an optimal choice can be made, because the eigenfunction $\hat{\psi}_2^o$ has been approximated. Thus we propose to follow the approach of [42] and choose the o -values where $\hat{\psi}_2^o$ achieves a minimum and a maximum, respectively, as purely belonging to A and B . Typically, these are the states the are on the left and the right boundary of the histogram in o . This approach will only start to give a biased estimate when the overlap of the A and B densities is so large that not even these extreme points are pure (see Fig. 2III, last row for such an example).

Let $\hat{\psi}_2$ be the second eigenvector of the Markov model $\mathbf{T}(\tau)$ of the finely binned observable (Eq. (36)). Then, $\hat{\psi}_2$ is a discrete approximation to the projected eigenfunction $\hat{\psi}_2^o$. Following the derivation given in the SI, the fuzzy membership functions on the discretized observable space are given by

$$\hat{\chi}_{A,i} = \frac{\max_j \hat{\psi}_{2,j} - \hat{\psi}_{2,i}}{\max_j \hat{\psi}_{2,j} - \min_j \hat{\psi}_{2,j}} \quad (44)$$

$$\hat{\chi}_{B,i} = \frac{\hat{\psi}_{2,i} - \min_j \hat{\psi}_{2,j}}{\max_j \hat{\psi}_{2,j} - \min_j \hat{\psi}_{2,j}}. \quad (45)$$

where the subscripts i and j denote the discrete state index. Note that the extreme values $\max_j \hat{\psi}_{2,j}$ and $\min_j \hat{\psi}_{2,j}$ may have large statistical uncertainties, when a fine and regular binning is used to discretize the observation. In order to avoid our estimates to be dominated by statistical fluctuations, we choose the outer most discretization bins such at at least least 0.05% of the total collected data is in each of them. The exact choice of this value appears to be irrelevant—as shown in the SI, any choice between 0.005% and 5% of the data yields similar results. Since we are restricted to the projected eigenfunction $\hat{\psi}_2$, we can determine the optimal choice $\hat{\chi}_A(o)$ and $\hat{\chi}_B(o)$ from $\hat{\psi}_2(o)$.

Together with the estimated stationary density $\mu^o(o)$ which can, e.g., be obtained by computing a histogram from sufficiently long equilibrium trajectories, the probability of being in A and B is thus given by:

$$\pi_A = \sum_i \mu_i^o \hat{\chi}_{A,i} \quad (46)$$

$$\pi_B = \sum_i \mu_i^o \hat{\chi}_{B,i} = 1 - \pi_A. \quad (47)$$

These probabilities can be used to split $\hat{\kappa}_2$ into micro-

scopic transition rates k_{AB} and k_{BA} :

$$\hat{k}_{AB} = \pi_B \hat{\kappa}_2 \quad (48)$$

$$\hat{k}_{BA} = \pi_A \hat{\kappa}_2 \quad (49)$$

Note that the assignment of labels “ A ” and “ B ” to parts of state space is arbitrary. Eq. (48) is the transition rate from A to B as defined by Eqs. (44)-(45), and Eq. (49) is the corresponding transition rate from B to A .

Spectral estimation procedure

The optimal estimator for κ_2 is thus one that fits the exponential decay of $\hat{\lambda}_2(\tau)$ while minimizing the fitting error Eq. (30). As analyzed above, the systematic fitting error is minimized by any multi- τ estimator. In order to obtain a numerically robust fit, especially in the case when statistical noise is present, it is optimal to fit to an autocorrelation function $\tilde{\lambda}_2(\tau)$ where the relevant slowest decay has maximum amplitude $\hat{\alpha}_0$. This is approximately achieved by constructing a fine discretization MSM on the observed coordinate (see Section “Optimal choice of $\hat{\psi}_2$ ”). Thus, the optimal estimator of κ_2 proceeds as outlined in (1-4) below. The full spectral estimation algorithm (1-6) additionally provides estimates for the microscopic rates k_{AB} , k_{BA} , and for the partial densities μ_A and μ_B :

1. Obtain a fine discretization of the observed coordinate o into n bins, say $[o_i, o_{i+1}]$ for $i \in 1 \dots n$. When using an equidistant binning make sure to increase the outer most states to a size to cover a significant part (e.g. 0.05%) of the total population.
2. Construct a row-stochastic transition matrix $\mathbf{T}(\tau)$ for different values of τ . The estimation of transition matrices from data have been described in detail [14]. A simple way of estimating $\mathbf{T}(\tau)$ is the following: (i) for all pairs i, j of bins, let $c_{ij}(\tau)$ be the number of times the trajectory has been in bin i at time t and in bin j at time $t + \tau$, summed over all time origins t ; (ii) estimate the elements of $\mathbf{T}(\tau)$ by $T_{ij}(\tau) = c_{ij}(\tau) / \sum_k c_{ik}(\tau)$. A numerically superior approach is to use a reversible transition matrix estimator [14].
3. Calculate the discrete stationary probability μ and the discrete eigenvector $\hat{\psi}_2$ by solving the eigenvalue equations:

$$\mathbf{T}^T(\tau) \mu = \mu \quad (50)$$

$$\mathbf{T}(\tau) \hat{\psi}_2 = \hat{\lambda}_2 \hat{\psi}_2 \quad (51)$$

with the largest eigenvalues $\lambda_1 = 1 < \hat{\lambda}_2 \leq \hat{\lambda}_3$. \mathbf{T}^T denotes the transpose of the transition matrix. The i -th element of the vectors μ and $\hat{\psi}_2$ approximate the stationary density $\mu(o)$ and $\hat{\psi}_2$ on the respective point $o = \frac{o_i + o_{i+1}}{2}$. Functions $\mu^o(o)$ and $\psi_2^o(o)$ can be obtained by some interpolation method.

4. Estimate the relaxation rate $\hat{\kappa}_2$ and the OQ $\hat{\alpha}$ via an exponential fit of $\alpha e^{-\kappa_2 \tau}$ to the tail of $\hat{\lambda}_2(\tau) = \langle \hat{\psi}_2(t) \hat{\psi}_2(t + \tau) \rangle_t$.
5. Calculate the partial densities μ_A and μ_B from Eqs. (46) and (47) using transition matrix eigenvectors estimated at a lag time τ_{min} at which the rate estimate $\hat{\kappa}_2$ is converged.
6. Calculate the microscopic transition rates k_{AB} and k_{BA} from Eqs. (48) and (49)

Note that this estimator is optimal in terms of minimizing the systematic error. When dealing with real data, the amount of statistics may set restrictions of how fine a discretization is suitable and how large a lag time τ will yield reasonable signal to noise. For a discussion of this issue refer to e.g., Ref. [36].

Illustrative two-state example

To illustrate the theory and the concepts of this paper, we compare the behavior of different order parameters, measurement noise and different estimators in Fig. 2. The full-space model here is a two-dimensional model system using overdamped Langevin dynamics in a bistable potential. This choice was made because the exact properties of this system are known and the quality of different estimates can thus be assessed. The potential is chosen such that the eigenfunction associated with the slow process, $\psi_2(x)$ varies in x_1 and is constant in x_2 , such that the choice $o = x_1$ represents a perfect projection and the choice $o = x_2$ represents the worst situation in which the slow process is invisible.

Fig. 2 shows three scenarios using

- I. $y = x_1$
(perfect order parameter — projection angle 0°),
- II. $y = \frac{1}{2}(x_1 + x_2)$
(average order parameter - projection angle 45°),
and
- III. $y = \frac{1}{4}(x_1 + 3x_2)$
(poor order parameter — projection angle 72°).

Additionally, we compare the results when the order parameter y is traced without noise (left half of panels 3-5), and when measurement noise is added (right half of panels 3-5). Noise here consists of adding a uniformly distributed random number from the interval $[-1,1]$ to the signal, such that the noise amplitude is roughly 25% of the signal amplitude.

Fig. 2, panels 2 show the apparent stationary density in the observable y , $\mu^y(y)$, or in the noisy observable o , $\mu^o(o)$, as a black solid line. The partial densities of sub-states A (orange) and B (grey) which comprise the total stationary density are shown as well. The lower part of the figure shows the observed eigenfunction associated

with the two-state transition process (ψ_2^y or ψ_2^o) as black solid line with grey background. For comparison the results in the case of noise are shown in the background with lighter colors. It is apparent that when the quality of the observation is reduced, either by choosing a poor order parameter, or by adding experimental noise, the overlap of the partial densities increases and the continuous projected eigenfunction ψ_2^o becomes smoother and thus increasingly deviates from the dividing surface model which is a step function switching at the dividing surface (dashed line).

Panels 3 show the estimation qualities or observation qualities (OQ) in these different scenarios. The fact that the green and red lines are approximately constant after $\tau = 5$ (when the fast processes have relaxed) shows that the OQ can be reliably estimated at these lag time ranges using either the dividing surface or the spectral estimation approach. The red line (spectral estimation) corresponds to the OQ, which varies between 1 (perfect order parameter I) and 0.15 (poor order parameter III with additional measurement noise). It is seen that the OQ given by the spectral estimator can be much larger than the suboptimal estimation quality of the dividing surface estimator that uses a fit to the number correlation function Eq. (24) (green line). This is especially apparent in the case of an intermediate-quality order parameter (Fig. 2II-3).

Panels 4 show the estimate of the relaxation rate κ_2 obtained for the three scenarios where each panel compares 5 different rate estimators with the exact result (black solid line): (1) Direct counting of transitions from time-filtered data (TST estimate, blue line). For this estimator, the x-axis denotes the length of the averaging window W , ranging from 1 to 100 frames. (2,3) The dividing surface estimates using either a single- τ estimator (28) (dashed green line), and the multi- τ estimator (solid green line). (4,5) The single- τ MSM estimate (dashed red line), and the multi- τ MSM estimate (spectral estimation, solid red line). For the single- τ and the exact estimators the x-axis indicates the used lag time τ in the estimation where for the multi- τ estimators (i.e., dividing surface and spectral estimation), the x-axis specifies τ which is the start of the time range $[\tau, \tau + 10]$ used for an exponential fit.

In the case of a perfect order parameter (I), all estimators yield the correct rate at lag times $\tau > 5$ time steps (where the fast processes with rates κ_3 or greater have disappeared). Only in the case of TST (blue line) with increasing size W of the filtering window, the estimated rate tends to be too slow because an increased number of short forward-and-backward transition events become smeared out by the filtering window, therefore systematically underestimating the rate. For the perfect order parameter I, the noise has little effect on the estimate, because the partial densities of states A and B are still well separated.

For the average-quality and poor order parameters, the MSM estimate breaks down dramatically, provid-

ing a strongly overestimated rate for $0 < \tau < 100$ time steps. Panels II-4 and III-4 show the typical behavior of the τ^{-1} -convergence of the MSM estimate predicted by the theory (Eq. (29)). Clearly, the MSM estimate will converge to the true value for very large values of τ , but especially for the situation of a poor order parameter, the minimal τ required to obtain a small estimation error is larger than the timescale κ_2^{-1} of the slowest process, thus rendering a reliable estimation impossible.

It is seen that the magnitude of the error for a given value of τ increases when either adding noise (left half of panels 4 vs right half) or decreasing the quality of the order parameter (panel II-4 vs panel III-4). This is because in this sequence the OQ deteriorates, as predicted by the theory of reaction coordinate qualities (see above), and hence the prefactor of the MSM error increases (see Eq. (29)).

As predicted by Eq. (31), the multi- τ estimators (dividing surface and spectral estimate, red and green solid lines) are always better than the single- τ estimates (red and green dashed lines). As predicted by Eq. (30), both the dividing surface and spectral estimate of $\hat{\kappa}_2$ converge when the fast processes have died out (here approximately at $\tau > 5$ time steps). Also, panels II-4 and III-4 show that the spectral estimate is more stable than the dividing surface estimate, i.e., it exhibits weaker fluctuations around the true value κ_2 . This is because the spectral estimate uses the OQ $\hat{\kappa}_0$ as estimation quality, which is larger than the estimation quality of other estimators, and thus the exponential tail of the autocorrelation function can be fitted using a larger amplitude of the process relaxation with rate κ_2 , achieving a better signal-to-noise ratio.

Panels 5 show the results of the microscopic rate k_{AB} that quantifies the rate at which rare transition events between the large (orange) state A and the smaller (gray) state B . The solid lines indicate the estimates from Eq. (48) either using the partial densities from the dividing surface (green), or PCCA+ (spectral estimate, red). For corresponding rates computed from a MSM using the different projections are shown in dashed lines. As expected, the partial densities from the dividing surface estimate are significantly biased as soon as the states overlap in the observable, either due to choosing a poor order parameter, or to experimental noise. As a result, the dividing surface estimates for the microscopic rates k_{AB} and k_{BA} are biased for all these cases (panels II-5, panels III-5). The spectral estimate gives an unbiased estimate for average overlap (panels II-5). For strong overlap, even the spectral estimator has a small bias because no pair of observable states can be found that are uniquely assignable to states A and B . Still, the spectral estimator yields good results even in the poor order parameter setting (panel III-5). Like for the relaxation rate (κ_2) estimate, the spectral estimator exhibits less fluctuations here because the larger estimation quality yields a better signal-to-noise ratio.

Applications to optical tweezer data

In order to illustrate the performance of spectral estimation on real data, it is applied to optical tweezer measurements of the extension fluctuations of two biomolecules examined in a recent optical force spectroscopy study: the p5ab RNA hairpin [44] and the H36Q mutant of sperm whale apo-myoglobin at low pH [45]. The p5ab hairpin forms a stem-loop structure with a bulge under native conditions (Fig. 3-1) and zips/unzips repeatedly under the conditions used to collect data (Fig. 3-2a), while apo-myoglobin (crystal structure shown in Fig. 3-4) hops between unfolded and molten globule states at the experimental pH of 5 (Fig. 3-5a) [45].

Experimental force trajectory data were generously provided by the authors of Refs. [44, 45]. Experimental details are given therein, but we briefly summarize aspects of the apparatus and experimental data collection procedure relevant to our analysis.

The instrument used to collect both datasets was a dual-beam counter-propagating optical trap [46]. The molecule of interest was tethered to polystyrene beads by means of dsDNA handles, with one bead suctioned onto a pipette and the other held in the optical trap. A piezoactuator controlled the position of the trap and allowed position resolution to within 0.5 nm, with the instrument operated in passive (equilibrium) mode such that the trap was stationary relative to the pipette during data collection. The force on the bead held in the optical trap was recorded at 50 kHz, with each recorded force trajectory 60 s in duration.

It is common practice to estimate rates in such data by directly counting the number of transitions across some user-defined dividing surface, and dividing by the total trajectory length. Often, this procedure is applied after filtering the data with a time-running average. The results of this common procedure (effectively a TST estimate, or an MSM estimate with $\tau = 1$), is shown in Figs. 3-3,6 (blue line) using various averaging window sizes W , and compared to the optimal estimator (spectral estimation) for a range of estimation lag times τ . Although the TST estimate shows less fluctuations the spectral estimation result converges much faster and provides a more stable result in terms of the varying parameter (lag time τ / window size W). TST also tends to underestimate the true rate for large window sizes W . Moreover, the TST estimate never shows any plateau, thereby making it impossible to decide which rate estimate should be used.

p5ab RNA Hairpin analysis

Fig. 4 compares the results of several rate estimators for optical tweezer measurement of the p5ab RNA hairpin extension fluctuations. A sketch of the RNA molecule and the experimental trajectory analyzed can

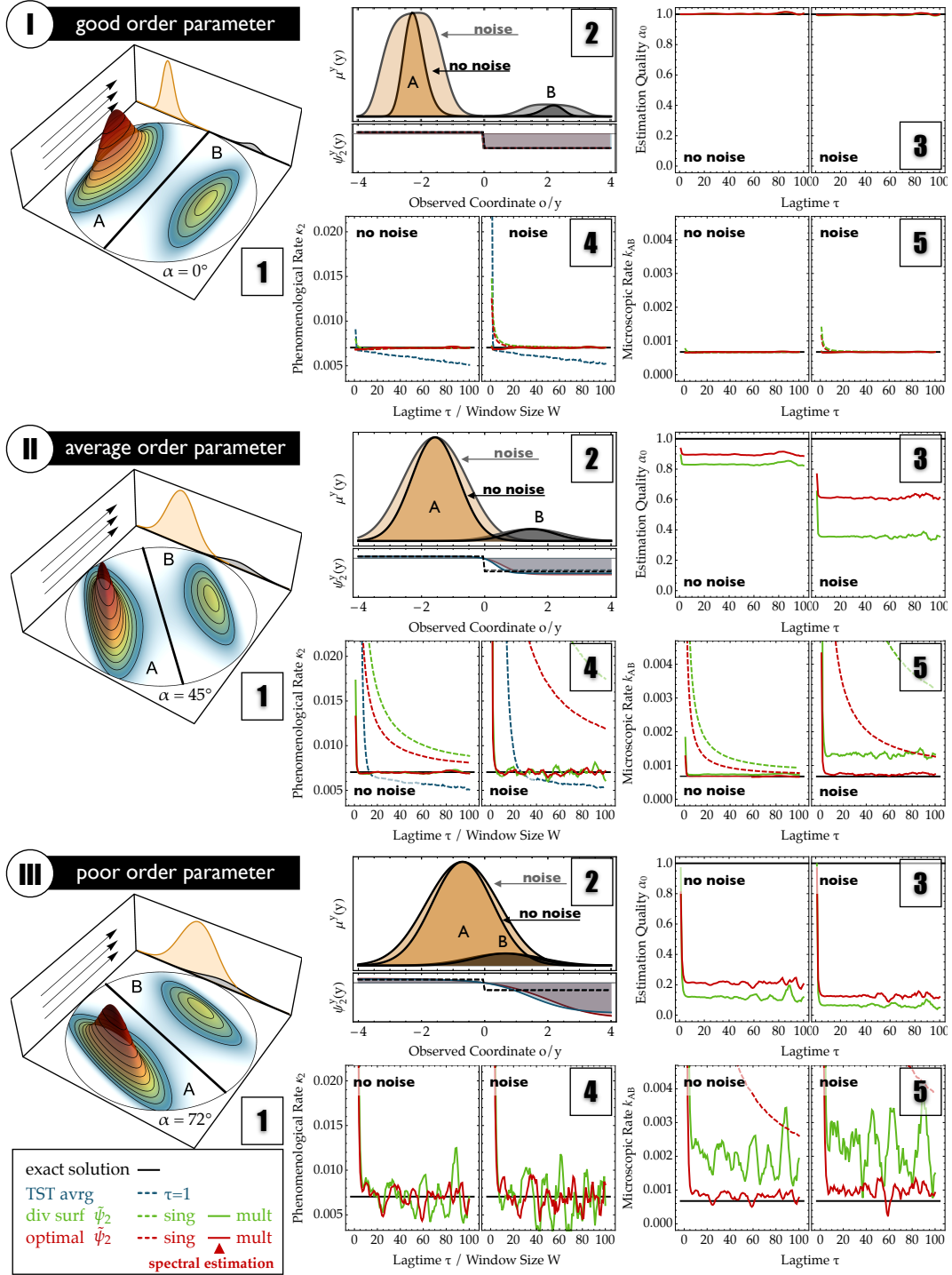


Figure 2. Estimation results using overdamped Langevin dynamics in a two-dimensional two-well potential that is projected onto different observables: (I) perfect projection, (II) average-quality projection, (III) poor projection. Results are compared without noise (left half of panels) and with additional measurement noise (right half of panels). (1) Full state space with indicated direction of the used order parameter. (2) (top) Stationary density $\mu^y(y)$ in the observable of the two partial densities of states A (orange) and B (gray). Results with noise are shaded lighter and are more spread out. (bottom) Second eigenvector without noise (solid, blue), with noise (solid, red) and dividing surface (black, dashed). (3) Estimation quality α from spectral estimation (OQ, red), and from exponential fitting to the number correlation function using a dividing surface at $y = 0$ (green). (4) Estimated relaxation rate κ_2 : TST with averaging window of size W (indicated in the x-axis). Dividing surface at $o = 0$ with single- τ (dashed green line) and multi- τ (solid green line) estimators. Estimates from an MSM-derived second eigenvector $\tilde{\psi}_2$ with a single- τ estimate (normal MSM, dashed red line), and multi- τ estimate (spectral estimation, solid red line). The black line is the reference solution, obtained from a direct MSM estimate for $\tau = 50$ in row 1. (5) The transition rates k_{AB} from state A to B. The coloring is identical to panels (4).

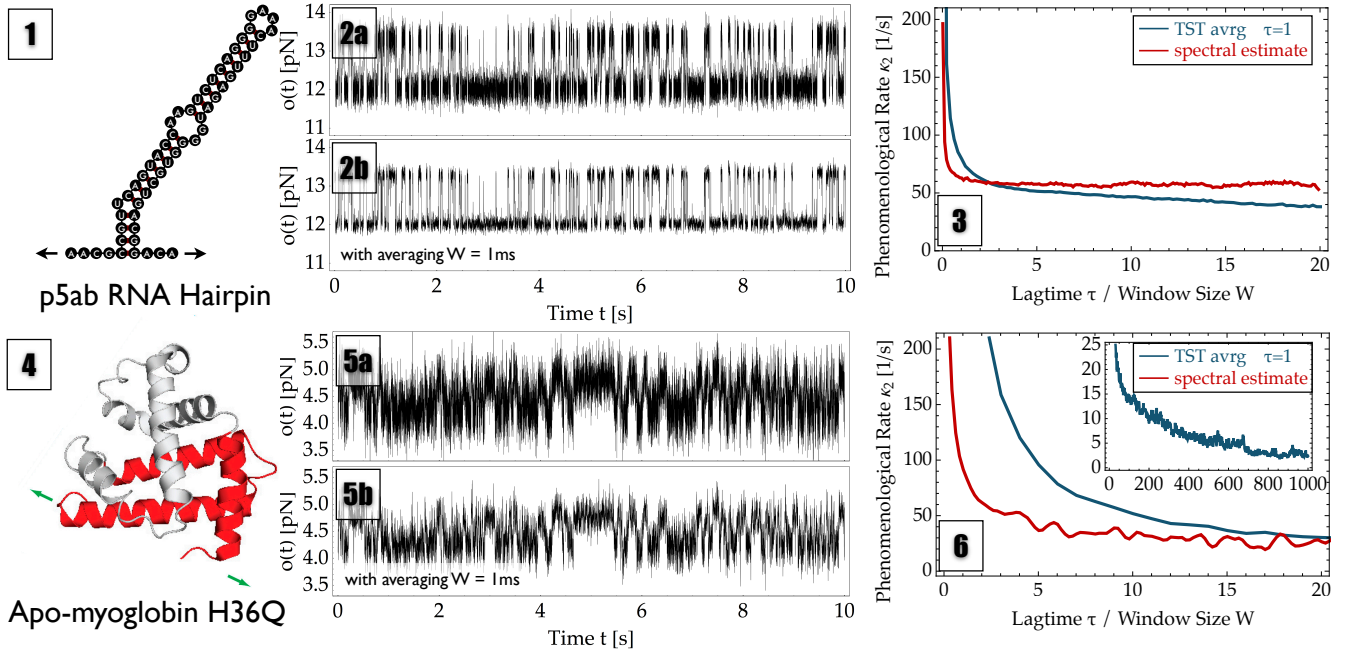


Figure 3. Probed systems by optical tweezer experiments: (top) RNA hairpin p5ab, (bottom) H36Q mutant of sperm whale apo-myoglobin. Panels (1,4) show schematic views of the probed system in its native secondary/tertiary structure including the direction of the pulling force (green and black arrows). Panels (2,5) show the traces used for analysis. Row (a) reports the results when directly analyzing the measured 50 kHz data, while row (b) reports the results when analyzing data that has been binned to 1 kHz to reduce the noise amplitude. Panel (3,6) show the estimated phenomenological rates $\hat{\kappa}_2$ for TPT (blue) using different averaging window sizes W (x-axis) and spectral estimation (red) for different lag times τ (x-axis). For apo-myoglobin the inset displays the long-behavior of TST at large window sizes W , where the rate is systematically underestimated.

be found in Fig. 3-1,2 top. The trajectory exhibits a two-state like behavior with state lifetimes on the order of tens of milliseconds. Fig. 4-1a shows the stationary probability density of measured pulling forces, exhibiting two nearly separated peaks. Fig. 4-2a shows the estimation quality α_o (OQ $\hat{\alpha}_o$ for the spectral estimator), which is approximately constant at lag times $\tau > 5$ ms, indicating a reliable estimate for this quantity at lag times greater than 5 ms. An optimum value of $\hat{\alpha}_o \approx 0.96$ (spectral estimator) is found while the best possible dividing surface results in $\alpha_o \approx 0.94$. These values indicate that the present reaction coordinate is well suited to separate the slowly interconverting states, and that different approaches, including a Markov model, a dividing surface estimate and a spectral estimate should yield good results.

Fig. 4-3a compares the estimates of the relaxation rate κ_2 using the direct MSM estimate (black), a fit to the fluctuation autocorrelation function using a dividing surface at the histogram minimum $o = 12.80$ pN (green), and spectral estimation (red). For the multi- τ estimators (dividing surface and spectral estimation), the lag time τ specifies the start of a time range $[\tau, \tau + 2.5$ ms] that was used for an exponential fit. All estimators agree on a relaxation rate of about $\hat{\kappa}_2 \approx 58$ s $^{-1}$, corresponding to a timescale of about 17 ms. The MSM estimate is strongly biased for short lag times, exhibiting the slow τ^{-1} con-

vergence predicted by the theory for single- τ estimators (Eq. (29)). It converges to an estimate within 10% of the value from multi- τ estimates after a lag time of about 10 ms. The dividing surface and spectral estimators behave almost identical, and converge after about $\tau = 5$ ms. According to the error theory of multi- τ estimators (Eq. (30)), this indicates that there are additional, faster kinetics in the data, the slowest of which have timescales of 2 – 3 ms. In agreement with the theory (Eq. (31)), the multi- τ estimators (dividing surface, spectral estimate) converge faster than the single- τ estimate (MSM).

As indicated in Fig. 4-1a, the substates estimated from PCCA+ are almost perfectly separated and can be well distinguished by a dividing surface at the histogram minimum $o = 12.80$ pN. Consequently, both the dividing surface estimate and the spectral estimate yield almost identical estimates of the microscopic transition rates — the folding rate being $k_{AB} \approx 45$ s $^{-1}$ and the unfolding rate being $k_{BA} \approx 15$ s $^{-1}$ (Fig. 4-4). In summary, the two-state kinetics of p5ab can be well estimated by various different rate estimators because the slowly-converting states are well separated in the experimental observable.

Fig. 4 panels b show estimation results for data that has been filtered by averaging over 50 frames (1 ms). This averaging further reduces the already small over-

lap between substates A and B while the filter length is much below the timescale of $A - B$ interconversion. Therefore, filtering has a positive result on the analysis: The effective OQ $\hat{\alpha}_o$ increases and is now approximately equal to 1 according to spectral estimation. The estimation results are largely identical to the case with noise. In Fig. 4-3b, the error made by the Markov model estimate has become smaller because the error prefactor reported in Eq. (29), $\ln \alpha_o$, has become smaller. Note that in contrast to the unfiltered data analysis, some of the rate estimates (MSM and spectral estimate) underestimate the rate for small lag times τ . This is not in contradiction with our theory which predicts an overestimation of the rate for Markovian processes. By using the filter, one has effectively introduced memory into the signal, and the present theory will only apply at a lag time τ that is a sufficiently large multiple of the filter length, such that the introduced memory effects have vanished.

Apo-myoglobin analysis

Fig. 5 shows estimation results for an optical tweezer experiment that probes the extension fluctuations of apo-myoglobin [47]. Fig. 3-4 shows a sketch of the experimental pulling coordinate (green arrows) depicted at the crystal structure of apo-myoglobin. Fig. 3-5 shows the trajectory that was analyzed. Out of the trajectories reported in [47] we have here chosen one where the two slowest-converting states have a large overlap. While the trajectory indicates that there are at least two kinetically separated states, the stationary probability density of measured pulling forces (Fig. 5-1a) does not exhibit a clear separation between these states in the measured pulling force. This is also indicated by Fig. 5-2a, which shows that the optimal observation quality (OQ) has a value of $\hat{\alpha}_o \approx 0.5$ (spectral estimator) at $\tau = 15$ ms while the best possible dividing surface results only yield an estimation quality of $\alpha_o \approx 0.4$ at $\tau = 15$ ms. Thus, the quality of the apo-myoglobin data is similar to that of the two-state model with intermediate-quality order parameter and noise (Fig. 2II-b). This data thus represents a harder test for rate estimators than the p5ab hairpin and should show differences between different rate estimators.

Fig. 5 panels 3 and 4 compare the estimates of κ_2 from the direct MSM estimate (black), a fit to the fluctuation autocorrelation function using a dividing surface at the local histogram maximum (minimum between two maxima with filtering) of the binned data at $o = 4.6$ pN (green), and spectral estimation (red). For the multi- τ estimators (dividing surface and spectral estimation), the lag time τ specifies the start of a time range $[\tau, \tau + 2.5$ ms] that was used for an exponential fit.

Fig. 5-3a shows again, that the MSM estimate of κ_2 exhibits the slow τ^{-1} convergence predicted by the theory (Eq. (29)) and does not yield a converged estimate using lag times of up to 20 ms. Since the MSM estimate still sig-

nificantly overestimates the rate at $\tau = 50$ ms when the relaxation process itself has almost entirely decayed, this estimator is not useful to analyze the apo-myoglobin data. In contrast, both, the dividing surface multi- τ approach and the spectral estimator do yield a converged estimate of $\hat{\kappa}_2 \approx 26$ s $^{-1}$, corresponding to a timescale of about 38 ms (Fig. 5-3a). In Ref. [47] a Hidden Markov model with Gaussian output functions was used and the rate was estimated to be $\hat{\kappa}_2 \approx 46$ s $^{-1}$ corresponding to a timescale of approximately 21 ms. These differences are consistent with our theory which shows that rate estimation errors lead to a systematic overestimation of the rate (and underestimation of the timescale). Fig. 5-1a shows the possible reason why the Gaussian HMM in [47] yields a rate overestimate: the partial probabilities are clearly not Gaussians. Following our theory, the smallest rate estimates the best estimates, which are here provided by the multi- τ estimators using either dividing surface or spectral estimation approaches.

In agreement with the theory (Eq. (31)), the multi- τ estimators (dividing surface, spectral estimate) converge faster than the single- τ estimate (MSM). A double-exponential fit to the spectral estimation autocorrelation function yields an estimate of $\kappa_3 \approx 100$ s $^{-1}$, corresponding to a timescale of 10 ms. Thus there is a timescale separation of a factor of about 4 between the slowest and the next-slowest process, indicating that when viewed at sufficiently large timescales (> 20 ms), the dynamics can be considered to be effectively two-state. However, since the present of faster processes is clearly visible in the data, it may be worthwhile to investigate further substates of the A and B states with multistate approaches such as Hidden Markov Models [23] or pair correlation analysis [27]. Such an analysis is beyond the scope of the present paper on two-state rate theory.

As indicated in Fig. 5-1a, the substates A and B estimated from PCCA+ do strongly overlap. Thus, even though the dividing surface estimator can recover the true relaxation rate κ_2 , the estimated microscopic rates k_{AB} and k_{BA} depend on the choice of the position of the dividing surface. Fig. 5-4a shows the estimates the dividing surface multi- τ estimator, evaluating to $k_{AB} \approx 12$ s $^{-1}$ and $k_{BA} \approx 15$ s $^{-1}$. In contrast, the spectral estimator yields estimates of $k_{AB} \approx 16$ s $^{-1}$ and $k_{BA} \approx 10$ s $^{-1}$. Although not being strongly different the diving surface approach suggests a reversed dominant direction of the process.

Like for the two-state model results shown in Fig. 2, the spectral estimate is numerically more stable in τ compared to the dividing surface estimate as a result of achieving a better signal-to-noise ratio. Clearly, in the dividing surface approach it is possible to pick a dividing surface position which yields the same estimates for k_{AB} and k_{BA} like the spectral estimator. However, the dividing surface estimator itself does not provide any information which is the correct choice, and therefore this theoretical possibility is of no practical use. Supplementary Figure 2 compares the estimation results of κ_2 and

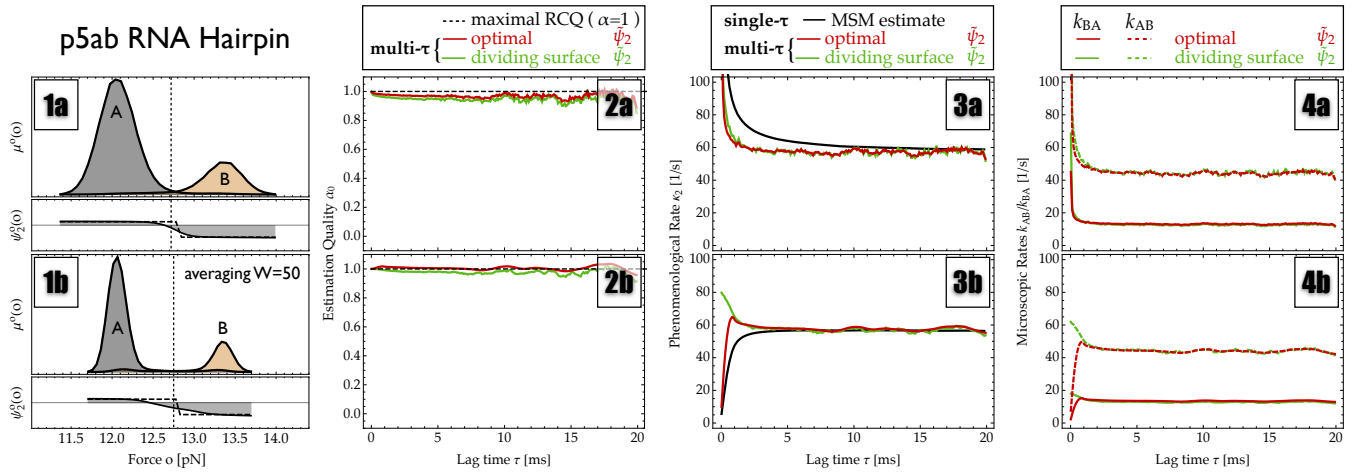


Figure 4. Estimates for rates and estimation qualities from passive-mode single-molecule force probe experiments of the p5ab RNA hairpin. All panels report the estimation results, showing the direct MSM estimate (black), a fit to the fluctuation autocorrelation function using a dividing surface at $o = 12.80$ pN (green), and spectral estimation (red). (1a+b): the stationary probability of observing a given force value (solid black line). The partial probabilities of states A (grey) and B (orange) obtained by spectral estimation show that there is very little overlap between the states. (2a+b): the estimation quality α_o , coinciding with the observation quality (OQ) $\hat{\alpha}_o$ for spectral estimation. (3a+b): estimated relaxation rate κ_2 . (4a+b): estimated microscopic transition rates: the folding rate k_{AB} (dashed) and the unfolding rate k_{BA} (solid).

k_{AB} , k_{BA} for different choices of the dividing surface. In contrast to the dividing surface approach, the spectral estimator only assumes that the extreme values of o are pure, which is a much weaker requirement than assuming that an appropriate dividing surface exists (see theory), and hence provides more reliable rate estimates.

The “b”-panels in Fig. 5 show the effect of filtering the data on the estimation results. Here, the data was averaged over a window length of 1 ms, corresponding to an averaging of 50 data points of the original 50 kHz data. Fig. 5-1b indicate that this filtering enhances the separation of states, and the apparent OQ increases to about $\hat{\alpha}_0 \approx 0.7$ (spectral estimate) while the dividing surface estimation quality is $\alpha_0 \approx 0.6$. The relaxation rate κ_2 is still estimated to have $\hat{\kappa}_2 \approx 26$ s⁻¹ and the estimate becomes more robust for both the dividing surface and spectral estimates (Fig. 5-3b). The MSM estimate slightly improves but is still significantly too high. Fig. 5-4b shows that the dividing surface derived rate estimates k_{AB} and k_{BA} have improved and are now similar to the spectral estimation results, while the spectral estimate itself remains at $k_{AB} \approx 16$ s⁻¹ and $k_{BA} \approx 10$ s⁻¹ independent of the filtering, which is in support of the reliability of the spectral estimate.

Summary

We have described a rate theory for observed two-state dynamical systems. The underlying system is assumed to be ergodic, reversible, and Markovian in full phase space, as fulfilled by most physical systems in thermal equilibrium. The observation process takes

into account that the system is not fully observed, but rather by tracing one order parameter (the extension to multiple order multidimensional order parameters is straightforward). During the observation process, the observed order parameter may be additionally distorted or dispersed, for example by experimental noise. Such observed dynamical systems occur frequently in the molecular sciences, and appear both in the analysis of molecular simulations as well as of single-molecule experiments.

The presented rate theory for observed two-state dynamics is a generalization to classical two-state rate theories in two ways: First, most available rate theories assume that the system of interest is either fully observable, or the relevant indicators of the slowest kinetic process can be observed without projection error or noise. Secondly, most classical rate theories are built on specific dynamical models such as Langevin or Smoluchowski dynamics. The present theory explicitly allows the two kinetic states to overlap in the observed signal (either due to using a poor order parameter or to noise broadening), and does not require a specific dynamical model, but rather works purely based on the spectral properties of a reversible ergodic Markov propagator — hence the name spectral rate theory.

Given the spectral rate theory, the systematic errors of available rate estimators can be quantified and compared. For example, the relatively large systematic estimation error in the implied timescales / implied rates of Markov state models is explained. Additionally, the theory provides a measure for the observation quality (OQ) $\hat{\alpha}_o$ of the observed signal, which is independent of any specific dynamical model and also does not need

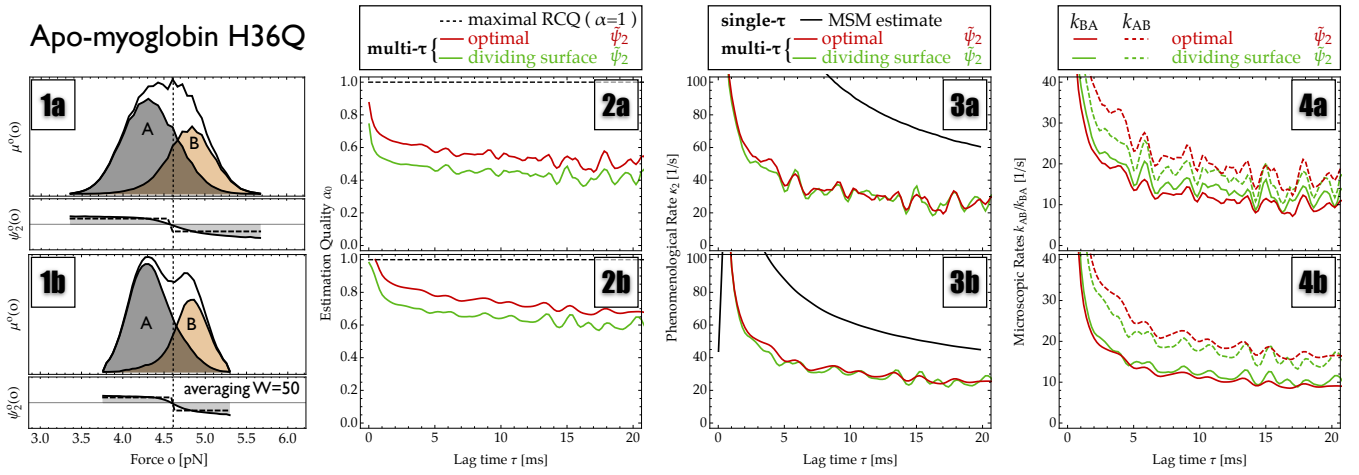


Figure 5. Estimates for rates and estimation qualities from passive-mode single-molecule force probe experiments of apo-myoglobin. All panels report the estimation results, showing the direct Markov model estimate (black), a fit to the fluctuation autocorrelation function using a dividing surface at the histogram maximum (minimum between two maxima for filtering) $o = 4.6$ pN (green), and spectral estimation (red). (1a+b): the stationary probability of observing a given force value (solid black line). The partial probabilities of states A (grey) and B (orange) obtained by spectral estimation show that there is very little overlap between the states. (2a+b): the estimation quality α_o , coinciding with the observation quality (OQ) $\hat{\alpha}_o$ for spectral estimation. (3a+b): estimated relaxation rate κ_2 . (4a+b): estimated microscopic transition rates k_{AB} (dashed) and k_{BA} (solid).

the definition of an “A” or “B” state and bounds the error in rates estimated from the observed signal. $\hat{\alpha}_o$ includes effects of the order parameter measured as well as the effect of the experimental construct on the signal quality, such as experimental noise. It is shown that $\hat{\alpha}_o$ is a lower bound to the true reaction coordinate quality (RCQ) due to choosing the order parameter, and can thus be used as an indicator to both improve the quality of the experimental setup and the choice of the order parameter.

The theory suggests steps to be taken to construct an optimal rate estimator, that minimizes the systematic error in the estimation of rates from an observed dynamical system. We propose such an estimator and refer to it as *spectral estimator*. It provides rather direct and optimal estimates for the following three types of quantities:

1. The observation quality (OQ) $\hat{\alpha}_o$ of the observed signal.
2. The dominant relaxation rate κ_2 , as well as the microscopic transition rates k_{AB} and k_{BA} , even if A and B strongly overlap in the observable.
3. The partial probability densities, and hence projections of the states A and B in the observable, $\mu_A^o(o)$ and $\mu_B^o(o)$, as well as their total probabilities, π_A and π_B . This information is also obtained if A and B strongly overlap in the observable.

Other rate estimators that rely on fitting the exponential tail of a time-correlation function calculated from the experimental recorded trajectories can also estimate

κ_2 without systematic error. However, the spectral estimator is unique in also being able to estimate k_{AB} , k_{BA} , $\mu_A^o(o)$, $\mu_B^o(o)$ and the OQ in the presence of states that overlap in the observable order parameter.

Discussion

The present study has concentrated on systematic rate estimation errors that are expected in the data-rich regime. We expect that taking the statistical error into consideration will make the spectral estimator described here even more preferable over more direct approaches such as fitting the number autocorrelation function of a dividing surface. This intuition comes from the fact that the spectral estimator maximizes the amplitude α with which the slow relaxation of interest is involved in the autocorrelation function. In the presence of statistical uncertainty, this will effectively maximize the signal-to-noise ratio in the autocorrelation function and thus lead to an advantage over fitting autocorrelation functions that were obtained differently.

Consideration of the statistical error will also aid in selecting an appropriate τ that balances systematic and statistical error in rate estimates. τ -dependent fluctuations of the sort observed in Fig. 2III-5 might also be suppressed by averaging over multiple choices of τ in a manner that incorporates the statistical error estimates in weighting.

The presented idea of building an optimal estimator for a single relaxation rate upon the transition matrix estimate of the projected slowest eigenfunction, $\hat{\psi}_2$, is

extensible to multiple relaxation rates, and this will be pursued in future studies.

Acknowledgements

The authors thank Susan Marqusee and Phillip J. Elms (UC Berkeley) for sharing the single-molecule force

probe data. FN and JHP acknowledge funding from the DFG center MATHEON. FN acknowledges funding from ERC starting grant “pcCell”. JDC acknowledges funding from a QB3-Berkeley Distinguished Postdoctoral Fellowship during part of this work. We are grateful to Christof Schütte, Attila Szabo, Sergio Bacallado, Vijay Pande and Heidrun Prantel for enlightening discussions and support.

-
- [1] William J. Greenleaf, Michael T. Woodside, and Steven M. Block. High-Resolution, Single-Molecule Measurements of Biomolecular Motion. *Annual Review of Biophysics and Biomolecular Structure*, 36(1):171–190, 2007.
 - [2] Lisa J. Lapidus, William A. Eaton, and James Hofrichter. Measuring the rate of intramolecular contact formation in polypeptides. *Proc. Natl. Acad. Sci. USA*, 97(13):7220–7225, June 2000.
 - [3] Huan-Xiang Zhou. Rate theories for biologists. *Quart. Rev. Biophys.*, 43, 2010.
 - [4] Olga K. Dudko, Thomas G. W. Graham, and Robert B. Best. Locating the barrier for folding of single molecules under an external force. *Phys. Rev. Lett.*, 107:208301, 2011.
 - [5] Greg Morrison, Changbong Hyeon, Michael Hinczewski, and D. Thirumalai. Compaction and tensile forces determine the accuracy of folding landscape parameters from single molecule pulling experiments. *Phys. Rev. Lett.*, 106:138102, 2011.
 - [6] H. Eyring. The activated complex in chemical reactions. *J. Chem. Phys.*, 3:107–115, 1935.
 - [7] David Chandler. Statistical mechanics of isomerization dynamics in liquids and the transition state approximation. *The Journal of Chemical Physics*, 68(6):2959–2970, 1978.
 - [8] John D. Chodera, Phillip J. Elms, William C. Swope, Jan-Hendrik Prinz, Susan Marqusee, Carlos Bustamante, Frank Noé, and Vijay S. Pande. A robust approach to estimating rates from time-correlation functions. <http://arxiv.org/abs/1108.2304>, 2011.
 - [9] Elliot L. Elson and Douglas Magde. Fluorescence Correlation Spectroscopy. I. Conceptual Basis and Theory. *Biopolymers*, 13:1–27, 1974.
 - [10] James L. Skinner and Peter G. Wolynes. Relaxation processes and chemical kinetics. *J. Chem. Phys.*, 69:2143+, 1978.
 - [11] J. D. Chodera, W. C. Swope, J. W. Pitera, and K. A. Dill. Long-time protein folding dynamics from short-time molecular dynamics simulations. *Multiscale Model. Simul.*, 5:1214–1226, 2006.
 - [12] J. D. Chodera, K. A. Dill, N. Singhal, V. S. Pande, W. C. Swope, and J. W. Pitera. Automatic discovery of metastable states for the construction of Markov models of macromolecular conformational dynamics. *J. Chem. Phys.*, 126:155101, 2007.
 - [13] Frank Noé, Illia Horenko, Christof Schütte, and Jeremy C. Smith. Hierarchical Analysis of Conformational Dynamics in Biomolecules: Transition Networks of Metastable States. *J. Chem. Phys.*, 126:155102, 2007.
 - [14] Jan-Hendrik Prinz, Hao Wu, Marco Sarich, Bettina Keller, Martin Fischbach, Martin Held, John D. Chodera, Christof Schütte, and Frank Noé. Markov models of molecular kinetics: Generation and validation. *J. Chem. Phys.*, 134:174105, 2011.
 - [15] W. C. Swope, J. W. Pitera, and F. Suits. Describing protein folding kinetics by molecular dynamics simulations: 1. Theory. *J. Phys. Chem. B*, 108:6571–6581, 2004.
 - [16] Marco Sarich, Frank Noé, and Christof Schütte. On the approximation error of markov state models. *SIAM Multiscale Model. Simul.*, 8:1154–1177, 2010.
 - [17] Susanna Kube and Marcus Weber. A coarse graining method for the identification of transition rates between molecular conformations. *J. Chem. Phys.*, 126(2):024103+, 2007.
 - [18] Nicaolae V. Buchete and Gerhard Hummer. Coarse Master Equations for Peptide Folding Dynamics. *J. Phys. Chem. B*, 112:6057–6069, 2008.
 - [19] C. Schütte, F. Noé, J. Lu, M. Sarich, and E. Vanden-Eijnden. Markov state models based on milestoning. *J. Chem. Phys.*, 134:204105, 2011.
 - [20] Ginka S. Buchner, Ronan D. Murphy, Nicolae-Viorel Buchete, and Jan Kubelka. Dynamics of protein folding: Probing the kinetic network of folding–unfolding transitions with experiment and theory. *Biochimica et Biophysica Acta*, 1814:1001–1020, 2011.
 - [21] Lawrence R. Rabiner. *A tutorial on hidden markov models and selected applications in speech recognition*, pages 257–286. 1989.
 - [22] Sean A. McKinney, Chirlmin Joo, and Taekjip Ha. Analysis of Single-Molecule FRET Trajectories Using Hidden Markov Modeling. *Biophysical Journal*, 91(5):1941–1951, September 2006.
 - [23] John D. Chodera, Phillip Elms, Frank Noé, Bettina Keller, Christian M. Kaiser, Aaron Ewall-Wice, Susan Marqusee, Carlos Bustamante, and Nina Singhal Hinrichs. Bayesian hidden markov model analysis of single-molecule force spectroscopy: Characterizing kinetics under measurement uncertainty. <http://arxiv.org/abs/1108.1430>, 2011.
 - [24] Irina V. Gopich and Attila Szabo. Decoding the pattern of photon colors in single-molecule FRET. *The journal of physical chemistry. B*, 113(31):10965–10973, August 2009.
 - [25] Johannes Stigler, Fabian Ziegler, Anja Gieseke, J. Christof M. Gebhardt, and Matthias Rief. The complex folding network of single calmodulin molecules. *Science*, 334:512–516, 2011.
 - [26] Menahem Pirchi, Guy Ziv, Inbal Riven, Sharona Sedghani Cohen, Nir Zohar, Yoav Barak, and Gilad Haran. Single-molecule fluorescence spectroscopy maps the folding landscape of a large protein. *Nature Comms*, 2:493, 2011.
 - [27] Armin Hoffmann and Michael T. Woodside. Signal-pair correlation analysis of single-molecule trajectories. *Angew. Chem. Int. Ed.*, 50:12643–12646, 2011.
 - [28] F. Barra, M. Clerc, and E. Tirapegui. Detailed balance in non-equilibrium systems. *Dynam. Stab. Syst.*, 12:61–70,

- 1997.
- [29] C. Schütte, A. Fischer, W. Huisinga, and P. Deuffhard. A Direct Approach to Conformational Dynamics based on Hybrid Monte Carlo. *J. Comput. Phys.*, 151:146–168, 1999.
 - [30] Frank Noé and Feliks Nüske. A variational approach to modeling slow processes in stochastic dynamical systems. *ArXiv e-prints*, November 2012.
 - [31] M. Hinczewski, Y. von Hansen, and R.R. Netz. Deconvolution of dynamic mechanical networks. *Proc. Natl. Acad. Sci. USA*, 107:21493–21498, 2010.
 - [32] Yann von Hansen, Alexander Mehlich, Benjamin Pelz, Matthias Rief, and Roland R. Netz. Auto- and cross-power spectral analysis of dual trap optical tweezer experiments using bayesian inference. *Rev. Sci. Instrum.*, 83:095116, 2012.
 - [33] M. Hinczewski, J.C.M. Gebhardt, M. Rief, and D. Thirumalai. From mechanical folding trajectories to intrinsic energy landscapes of biopolymers. *Proc. Natl. Acad. Sci. USA*, 110:4500–4505, 2013.
 - [34] L. Onsager. Reciprocal relations in irreversible processes II. *Phys. Rev.*, 38:2265–2279, 1931.
 - [35] John A. Montgomery, David Chandler, and Bruce J. Berne. Trajectory analysis of a kinetic theory for isomerization dynamics in condensed phases. *The Journal of Chemical Physics*, 70(9):4056–4066, 1979.
 - [36] Robert Zwanzig and Narinder K. Ailawadi. Statistical Error Due to Finite Time Averaging in Computer Experiments. *Physical Review Online Archive (Prola)*, 182:280–283, June 1969.
 - [37] W. Ritz. Über eine neue methode zur lösung gewisser variationsprobleme der mathematischen physik. *J. Reine Angew. Math.*, 135:1–61, 1909.
 - [38] Baron Peters. Using the histogram test to quantify reaction coordinate error. *The Journal of Chemical Physics*, 125(24):241101+, 2006.
 - [39] Frank Noé, Christof Schütte, Eric Vanden-Eijnden, Lothar Reich, and Thomas R. Weigl. Constructing the full ensemble of folding pathways from short off-equilibrium simulations. *Proc. Natl. Acad. Sci. USA*, 106:19011–19016, 2009.
 - [40] Vincent A. Voelz, Gregory R. Bowman, Kyle Beauchamp, and Vijay S. Pande. Molecular Simulation of ab Initio Protein Folding for a Millisecond Folder NTL9. *J. Am. Chem. Soc.*, 132(5):1526–1528, February 2010.
 - [41] Gregory R. Bowman, Kyle A. Beauchamp, George Boxer, and Vijay S. Pande. Progress and challenges in the automated construction of Markov state models for full protein systems. *J. Chem. Phys.*, 131(12):124101+, September 2009.
 - [42] P. Deuffhard and M. Weber. Robust Perron cluster analysis in conformation dynamics. *ZIB Report*, 03-09, 2003.
 - [43] P. Deuffhard, W. Huisinga, A. Fischer, and C. Schütte. Identification of almost invariant aggregates in reversibly nearly uncoupled Markov chains. *Lin. Alg. Appl.*, 315:39–59, 2000.
 - [44] Phillip J. Elms, John D. Chodera, Carlos Bustamante, and Susan Marqusee. The limitations of constant-force-feedback experiments. *Biophys. J.*, 103:1490, 2012.
 - [45] Phillip J. Elms, John D. Chodera, Carlos Bustamante, and Susan Marqusee. The molten globule state is unusually deformable under mechanical force. *Proc. Natl. Acad. Sci. USA*, 109:3796, 2012.
 - [46] Carlos J. Bustamante and Steven B. Smith. Light-force sensor and method for measuring axial optical-trap forces from changes in light momentum along an optic axis, 2006.
 - [47] Phillip J. Elms, John D. Chodera, Carlos Bustamante, and Susan Marqusee. The molten globule state is unusually deformable under mechanical force. *Proc. Natl. Acad. Sci. USA*, 109:3796–3801, 2012.